

THE COSMIC RAY ENERGY SPECTRUM

FROM 2×10^{17} TO 10^{19} eV

by

Donald Robert Cady

A dissertation submitted to the faculty of
The University of Utah
in partial fulfillment of the requirements for the degree of

Doctor of Philosophy

Department of Physics

The University of Utah

August 1983

© 1983 D. Robert Cady

All Rights Reserved

THE UNIVERSITY OF UTAH GRADUATE SCHOOL

SUPERVISORY COMMITTEE APPROVAL

of a dissertation submitted by

Donald Robert Cady

This dissertation has been read by each member of the following supervisory committee and by majority vote has been found to be satisfactory.

July 21, 1983

Geo L Cassidy
Chairman: George L. Cassidy

July 21, 1983

Haven E Bergeson
Haven E. Bergeson

July 21, 1983

Donald E. Groom
Donald E. Groom

JULY 21, 1983

Frank E. Harris
Frank E. Harris

July 21, 1983

Owen W. Johnson
Owen W. Johnson

THE UNIVERSITY OF UTAH GRADUATE SCHOOL

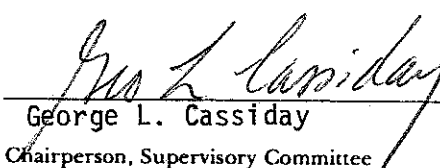
FINAL READING APPROVAL

To the Graduate Council of The University of Utah:

I have read the dissertation of Donald Robert Cady in its final form and have found that (1) its format, citations, and bibliographic style are consistent and acceptable; (2) its illustrative materials including figures, tables, and charts are in place; and (3) the final manuscript is satisfactory to the Supervisory Committee and is ready for submission to the Graduate School.

July 21, 1983

Date


George L. Cassidy

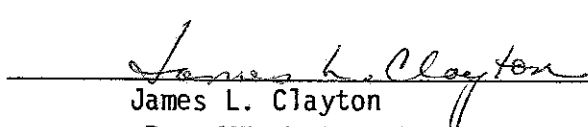
Chairperson, Supervisory Committee

Approved for the Major Department


Eugene C. Loh

Chairman / Dean

Approved for the Graduate Council


James L. Clayton

Dean of The Graduate School

THE COSMIC RAY ENERGY SPECTRUM

FROM 2×10^{17} to 10^{19} eV

by

Donald Robert Cady

An abstract of a dissertation submitted to the faculty of
The University of Utah
in partial fulfillment of the requirements for the degree of

Doctor of Philosophy

George Lawrence Cassiday

Chairman

Professor of Physics

Department of Physics

The University of Utah

August 1983

ABSTRACT

The Fly's Eye detector is designed to detect the fluorescence and Cherenkov light emitted as cosmic ray air showers traverse the atmosphere. The detector, which is located on top of Little Granite Mountain in the Dugway Army Proving Grounds, Utah, consists of 880 photomultiplier tubes arranged at the foci of 67 mirrors such that each phototube views a different part of the sky. Knowledge of the orientation of each phototube, and the times at which the pulses of light from the shower arrives at each phototube, allows one to reconstruct the geometry of an air shower. Knowledge of the integral of the light pulse, along with knowledge of the shower trajectory, allows one to determine the number of charged particles in the light emitting portion of the shower, giving the longitudinal development of the shower and therefore the energy of the primary cosmic ray that initiated the shower. In this paper, I discuss the theory of operation of the Fly's Eye, and report on the results of one experiment performed with it; the measurement of the integrated energy spectrum $I(>E)=AE^{-\gamma}$ in the energy range 2×10^{17} eV to 10^{19} eV by considering the distribution of events with respect to distance from the Fly's Eye. The analysis gives a spectral index (γ) of 1.99 ± 0.04 and a normalization (A) of $(1.92 \pm 0.12) \times 10^{-10} \text{ m}^{-2} \text{ s}^{-1} \text{ str}^{-1}$. This agrees well with the results of other groups working in the same energy range.

CONTENTS

| | |
|---|-----|
| ABSTRACT | iv |
| LIST OF FIGURES | vii |
| 1. INTRODUCTION | 1 |
| 2. THE NATURE OF COSMIC RAYS | 4 |
| 2.1 Properties | 4 |
| 2.1.1 Models of Origin | 4 |
| 2.1.2 Spectrum. | 9 |
| 2.1.3 Composition. | 13 |
| 2.2 Extensive Air Showers | 14 |
| 2.2.1 Shower Components. | 15 |
| 2.2.2 Light Output | 17 |
| 2.2.2.1 Cherenkov radiation. | 17 |
| 2.2.2.2 Scintillation light. | 18 |
| 2.3 Traditional Techniques for Detecting UHCR's | 18 |
| 2.3.1 Particle Detectors | 19 |
| 2.3.1.1 Electron detectors | 19 |
| 2.3.1.2 Muon detectors | 21 |
| 2.3.1.3 Hadron detectors. | 22 |
| 2.3.2 Atmospheric Cherenkov Detectors | 22 |
| 2.3.3 Present Detectors and Their Limitations | 23 |
| 3. THE FLY'S EYE | 26 |
| 3.1 Theory of Operation | 26 |
| 3.1.1 Gathering of Light | 26 |
| 3.1.2 Geometrical Reconstruction. | 27 |
| 3.1.3 Size Analysis | 33 |
| 3.2 The Detector | 33 |
| 3.2.1 Physical Layout | 33 |
| 3.2.2 System Overview | 44 |
| 3.2.2.1 Data Path | 44 |
| 3.2.2.2 Triggering. | 44 |
| 3.2.3 Software. | 45 |
| 3.2.3.1 Data Aquisition | 45 |
| 3.2.3.2 Calibration | 46 |
| 4. DATA ANALYSIS | 47 |
| 4.1 Scanning | 47 |
| 4.2 Geometrical Reconstruction | 47 |

| | | |
|-------|--|----|
| 4.3 | Binning of Reconstructed Events | 48 |
| 4.4 | Simulation of Detector Response | 49 |
| 4.4.1 | Simulation Geometry | 49 |
| 4.4.2 | Simulation Algorithm. | 52 |
| 5. | RESULTS | 56 |
| 5.1 | Raw Distributions | 56 |
| 5.2 | Simple Parametric Fit to Data | 56 |
| 5.3 | Simulation Fit | 68 |
| 5.4 | Comparison with Results of Others. | 68 |
| | LIST OF REFERENCES | 74 |

LIST OF FIGURES

| Figure | Page |
|--------|---|
| 1 | The Cosmic Ray Integral Energy Spectrum 10 |
| 2 | Reconstruction Geometry 28 |
| 3 | Tangent Plane Relative to Detector 31 |
| 4 | Aerial View of Detector 34 |
| 5 | Inside View of Mirror Housing 36 |
| 6 | Inside Trailer-Ommatidial Racks 38 |
| 7 | Inside Trailer-HV Racks and Back of Ommatidial Racks . 40 |
| 8 | Inside Trailer-Operator's Console and Event Display . 42 |
| 9 | Simulation Geometry 50 |
| 10 | Experimental Distribution Sample (a) 57 |
| 11 | Experimental Distribution Sample (b) 59 |
| 12 | Event with Cherenkov "Blast" at Beginning. 61 |
| 13 | Well Reconstructed Event 63 |
| 14 | Simple Parametric Fit to Sample (b) 66 |
| 15 | Simulation Fit to Sample (a) 69 |
| 16 | Simulation Fit to Sample (b) 71 |

CHAPTER 1

INTRODUCTION

Ever since Victor Hess proved the existence of cosmic rays during a balloon flight in 1912,¹ physicists have been studying them. Originally the term "cosmic ray" referred to a penetrating radiation of unknown composition which apparently originated from outside the atmosphere. Today we know that this radiation, which does indeed come from outer space, consists mostly of atomic nuclei with energies ranging from just above that of the solar wind (a distinction mostly of convenience) to 10^{20} eV, and perhaps higher, and some gamma rays and electrons (at the lower energies). We also now differentiate between the primary cosmic rays, which are the particles mentioned above, and the secondary cosmic rays, which are mostly electrons and muons. When a cosmic ray primary strikes the atmosphere, it interacts with the nucleus of an air molecule to create a shower of secondary particles. These secondaries in turn interact, creating more particles. As this shower of secondary particles traverses the atmosphere, the number of particles first increases, reaches a maximum, and then slowly decreases. It was these secondaries that Hess and other early workers detected. Except for some satellite and high altitude balloon experiments, it is still the secondaries that cosmic ray researchers investigate.

While much has been learned about cosmic rays in the last sev-

enty years, much remains to be explained. For instance, the exact composition of the primaries (which nuclei occur in the primaries and with what abundance) is only known at energies below about 10^{14} eV. Some models of acceleration and propagation of cosmic rays predict a changing composition around 10^{15} eV, but present observations do not allow us to say which models could be right. Also, efforts to examine elementary particle interactions at extremely high energies by examining the behavior of the showers started by ultra-high energy cosmic rays (or UHCR's) are hindered by this uncertainty of primary composition.

The energy spectrum of the cosmic rays is also of interest. The spectrum is fairly well known below 10^{16} eV, but there is a paucity of observations between 10^{16} and 10^{17} eV. Above 10^{17} eV, the rate at which cosmic rays arrive is so low, there are only a handful of detectors worldwide that are capable of collecting data on them. At even higher energies (above 3×10^{19} eV) the spectral data of different groups are contradictory, with some groups seeing the spectrum steepening above that energy, and some groups seeing it flattening. In this paper the term "energy spectrum" will refer to the integrated spectrum $I(>E) = A \cdot (E/10^{17} \text{ eV})^{-\gamma}$ where $I(>E)$ is the rate at which cosmic ray primaries of energy greater than E cross a unit area per unit time from a unit solid angle, A is a normalization factor, and γ is the "spectral index." When referring to the the spectrum "steepening" or "flattening," we will actually mean that the spectral index becomes larger or smaller. The integrated spectrum will be quoted because in measuring it one does not need to

know the energy of each individual shower that triggered one's detector. Instead, one only needs to know the minimum energy for such a shower to have triggered the detector, and the rate at which the triggers occurred. This minimum energy can be found by simulation and estimates of detector response.

This paper describes the theory and operation of the Fly's Eye, a new technique for measuring properties of cosmic ray showers that promises to provide valuable information necessary to resolve some of the above problems. The paper also give the results of one experiment performed with the Fly's Eye, the measurement of the integrated energy spectrum of the cosmic rays between 2×10^{17} and 10^{19} eV.

CHAPTER 2

THE NATURE OF COSMIC RAYS

2.1 Properties

2.1.1 Models of Origin

The search for sources of cosmic rays is complicated by the fact that the galactic magnetic fields bend the particles' trajectories so much that the direction the cosmic ray is traveling when it is detected often bears no relation to its initial direction of travel. Hence, the spatial distribution of low energy cosmic rays as measured at the earth is nearly isotropic with a small "forward-backward" intensity difference due partly to the motion of the earth through this low energy cosmic ray "gas." An additional anisotropy, due to the streaming of this gas along the galactic spiral arms, is expected to have an amplitude about the same order of magnitude as the above effects (this anisotropy can be likened to a "wind" of cosmic rays blowing along the spiral arms, in which each constituent particle moves randomly, as the gas as a whole moves along). Observations at about 10^{12} eV do show such an effect, albeit in an unexpected direction.² For cosmic rays with energies above about 10^{19} eV, the momenta of the particles are great enough that their trajectories through space are not bent appreciably. However, the intensity of these cosmic rays is very low; only thirty-two events with energies above 4×10^{19} eV have been collected world wide over the

the last twenty years.³ These ultra-high energy cosmic rays seem to come from the Virgo cluster of galaxies, but statistics are not good enough to be certain of this and the estimates of energy may be too high.⁴ Still, the existence of particles with roughly these energies places constraints on the possible models for origin of cosmic rays.

The earliest "successful" attempt to explain the origin of cosmic rays was Enrico Fermi's stochastic acceleration model.⁵ In this model, nuclei injected into interstellar space above a certain energy (the injection energy) could gain energy in collisions with moving magnetic clouds. These clouds are regions of higher than normal matter density that have a higher than normal magnetic field density due to magnetohydrodynamic effects. A cosmic ray particle would penetrate a cloud and then be expelled by the cloud's magnetic field. Since this would be an elastic collision, the particle would gain energy if the cloud were moving in the opposite direction to the particle's original direction, and lose energy if the cloud were moving in the same direction. Since, on the average, the particle would encounter more clouds moving in the opposite direction than in the same (for much the same reason that a car going down the highway passes more cars going in the opposite direction than in the same), over time the particle would gain energy.

This model predicted both the observed form for the energy spectrum (an inverse power law with the exponent in the vicinity of two) and the observed absence of high energy electrons (above a certain energy, the electrons would lose more energy to synchrotron

radiation while undergoing a "collision" with a magnetic cloud than they could gain in the collisions). However, there were some problems with the model.⁵ (For instance, the particles must be injected into interstellar space above a certain energy in order to have the gains in energy due to collisions be larger than the losses due to ionization. While this injection energy is quite modest for protons (about 200 MeV), it is sufficiently higher for heavy nuclei (on the order of tens of GeV) that one would expect an enhancement of protons over heavy nuclei. Yet up to about 10^{15} eV, heavy nuclei appear in cosmic rays in about the same proportions as they occur in normal interstellar matter, with some important exceptions.^{6,7}

Another problem with the model is related to the first. Compared to normal interstellar matter, cosmic rays have a small excess of certain light nuclei (^3He , ^7Li , Be, B).⁸ These nuclei are practically nonexistent in normal interstellar matter, because they are not created in abundance in normal stellar nucleosynthesis, as they are easily destroyed at stellar core temperatures. Their occurrence in cosmic rays can be explained by their production in the breakup of heavier nuclei in collisions with atoms of the interstellar medium. If one assumes that the original abundances of nuclei in the cosmic rays are the same as in stellar matter, one finds that they must have passed through about 5 gm/cm^2 of matter in order to yield the observed abundances.⁹ If the lower energy cosmic rays (upon whose abundances these calculations are based) are confined to the galaxy by the galactic magnetic fields, then this suggests (using the known density of interstellar matter) the lifetime of cosmic

rays is on the order of ten million years.¹⁰ Yet, according to Fermi,⁵ the time required for a particle to double its energy is also on the order of ten million years. Obviously, a more efficient acceleration mechanism is needed if these particles are to reach such high energies in such a short time.

Several present day theories seem to promise this. In the most popular theory, acceleration occurs in supernova shocks, where the expanding gaseous shell of a supernova, and its remnant magnetic field, are compressed at the interface with the interstellar medium.¹¹ A small acceleration of particles ("supra-thermal" particles) has been observed to occur at similar shocks where the magnetic fields of the earth and Jupiter have their interfaces with the solar wind. Reasonable estimates of the fields created at a supernova shock give rise to an energy spectrum similar to that observed below 10^{15} eV. Unfortunately, this mechanism seems to cut off above that energy. One possible solution to this problem is to further accelerate the particles with a "second-order" Fermi mechanism,¹² by using the remnants of old supernova shocks travelling through space as the magnetic clouds of the original Fermi mechanism. Other possible sources of secondary acceleration proposed are:¹² shocks about OB stars, which have especially strong stellar winds (also a candidate for injection); and acceleration by magnetohydrodynamic waves inside the supernova remnant. Note that whatever the final acceleration mechanism, initial acceleration in supernova shocks provides an efficient method of injection which overcomes the problems of accelerating heavy nuclei in models like Fermi's.¹³

Pulsars could be a source of high energy cosmic rays that would not require secondary acceleration. Some models predict electric potentials on the order of 10^{20} V near the surface of a pulsar. Pulsars should be about as plentiful as supernova shocks and should have the same spatial distribution, both being remnants of supernovae. However, no consistent model exists for the structure of pulsars, let alone for their acceleration mechanisms.¹⁴

Two other possible sources, black holes and Seyfert galaxies (which are thought by some to be galaxies with large black holes at their cores), are cited only because they seem to have enough energy to create the observed flux of high energy cosmic rays.^{15,16} There exists no generally accepted models for acceleration due to these objects since little observational evidence exists to use to construct such models.

Quasars are not thought to be significant sources because they are thought to be too far away in space. Particles with energies in excess of 6×10^{19} eV should theoretically lose energy through interactions with the 3° background radiation with an interaction length of about 20 Mpc.¹⁷ Since particles with energies above this are believed to have been seen, one would suspect that they must have traveled less than that distance (which is the distance to the Virgo cluster, a source of Seyfert galaxies). Therefore quasars, which are thought to be thousands of Mpc away, would not be likely sources of UHCR's. Even if they are close by (and recent evidence¹⁸ suggests they are not) the large red shifts of quasars would decrease the flux of UHCR's by about a factor of ten, which means quasars

would have to be very efficient sources. Of course, if the Yakutsk data on the UHCR spectrum is correct (see next section), this would not be a problem, because there essentially would be no UHCR's.

2.1.2 Spectrum

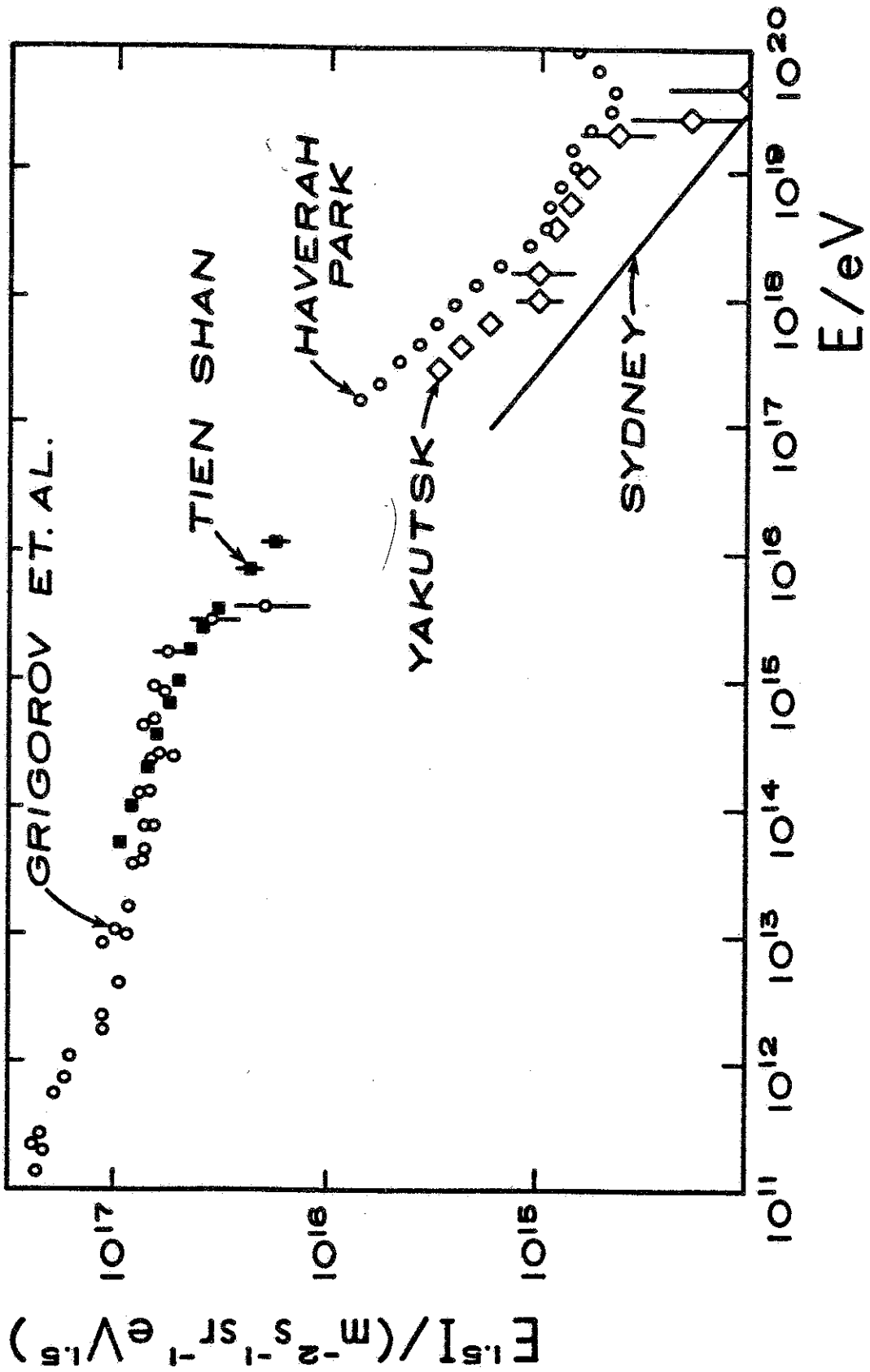
The present knowledge of the cosmic ray integrated energy spectrum is shown in Figure 1. The main features of interest are the "knee" at 10^{15} eV, and the "ankle" at about 4×10^{19} eV. The "knee," a steepening of the spectrum, is usually interpreted as representing the onset of escape from the galaxy of cosmic rays with rigidities[†] (momentum per unit charge) above 10^{14} V/c. At low energies the cosmic rays are effectively trapped in the galaxy by the galactic magnetic field. At higher energies, the trajectories of the cosmic rays are not bent as much by the magnetic field, and hence they are able to escape from the galaxy faster. With increasing energy the rate of escape increases until as many cosmic rays enter the galaxy from extra-galactic space as leave it. This is known as the "leaky box" model.¹⁹ This model predicts that (for a given energy) the percentage of heavy nuclei in the cosmic ray flux will be enhanced in the "knee" region. The heavy nuclei, with their larger charges, will have their trajectories bent more in the galactic magnetic field than protons and therefore will be trapped more effectively in the galaxy. Unfortunately, the available data on composition in this energy range are inconsistent.⁴ However, due

† A cosmic ray proton ($Z=1$) with a rigidity of 10^{14} V/c would have a momentum of 10^{14} eV/c. A cosmic ray iron nucleus ($Z=26$) with the same rigidity would have a momentum of 2.6×10^{15} eV/c.

FIGURE 1

The Cosmic Ray Integral
Energy Spectrum⁴

Note the breaks in the spectral slope at 10^{15} eV (the "knee")
and at 3×10^{19} eV (the "ankle").



to problems in observing cosmic rays in the energy range 10^{14} to 10^{17} eV, their properties are not yet well established.²⁰ The intensity of these particles is too low for their properties to be measured accurately by satellite or balloon borne detectors, while the air showers created by primaries of these energies are too small to be measured well by the larger ground-based detectors.

The "ankle" is even more mysterious. If UHCR's are universal, theory predicts the spectrum should cut off above about 6×10^{19} eV due to interactions with the 3° background radiation.¹⁷ If, on the other hand, they are produced in all galaxies, the spectrum should still steepen due to the UHCR's nearly unimpeded escape from our galaxy, provided that other galaxies have the same production spectra for UHCR's. While data from the array at Yakutsk²¹ tends to support the above expectations, data gathered by the array at Haverah Park²² (supported by data from Volcano Ranch) shows the spectrum instead flattening out above 3×10^{19} eV. This behavior may be due to a local source (within 20 Mpc) of UHCR's with a flat spectrum. If this is the case, we should see a marked anisotropy in the arrival directions of UHCR's. Current observations, however, suffer from the problem discussed in the previous section, poor statistics and possible bad estimates of energy (this is based on the same data). It should be noted that the Yakutsk group carried out an extensive set of intercalibrations of the several types of detectors that make up their array. Their estimates of shower energies should be the most accurate of all the big arrays. However, for energies below 10^{19} eV, the estimates used by the other groups seem to work

just as well.³ The reason for the discrepancy at higher energies is not understood at present. Obviously better statistics and a less model-dependent energy estimate are needed in this energy range.

2.1.3 Composition

In the energy range covered by this experiment (2×10^{17} to 10^{19} eV) the available information on composition is contradictory. Some possibilities can be ruled out. According to Linsley,²² primaries cannot be dust grains (showers start too deep in the atmosphere) or neutrinos (showers do not start deep enough in the atmosphere, also borne out by our own observations²³). Gamma rays would create showers with low numbers of muons and hadrons.²⁴ Since such showers are rarely observed, it can be deduced that gamma rays are not important constituents of cosmic rays. This is not to say that there are no neutrinos, relativistic dust grains or high energy gammas in the flux, only that they cannot be the main constituents (as a matter of fact, high energy gammas have been observed). Below 10^{14} eV, direct observations with balloon and satellite borne detectors show that the flux is mostly atomic nuclei. Theoretically, one would expect this, as the acceleration mechanism seems to be electromagnetic and the lightest and most abundant stable charged particles are the electron and the proton, with the electron being so light it easily loses energy by synchrotron radiation. The nuclei are mostly hydrogen (protons) with heavier nuclei occurring in about the same proportions as in normal interstellar matter. One would suppose that the primaries are still nuclei at higher energies, but

which nuclei? Some of the reasons for a changing composition at higher energies were discussed in the previous section. Linsley and Watson²⁵ argue for a composition of mainly heavy nuclei (iron and heavier) at 10^{16} eV, changing to mostly protons by 10^{18} eV from an analysis of elongation rate data[†]. A similar analysis carried out by Thornton and Clay,²⁶ using a different experimental technique to determine the depth of maximum, gave similar results. On the other hand, Gaisser et al.²⁷ argue for a composition of heavy nuclei from 10^{16} eV all the way up to 10^{18} eV (the data they worked with does not extend past that). They base this on computer simulations fitting the data on average shower development from the Chacaltaya experiment.^{§,28}

2.2 Extensive Air Showers

When a cosmic ray enters the atmosphere it interacts with the

† The elongation rate is the variation of depth of maximum development of the shower with energy. At a given energy, showers initiated by heavy nuclei develop faster than showers initiated by protons since to a good approximation, a shower initiated by a nucleus of mass N with energy E acts like N superimposed showers, each of energy E/N . According to the elongation rate theorem,²⁹ for a fixed composition the depth of maximum development should vary as the log of the primary's energy. If, following Linsley and Watson, one plots the actual variation of depth of maximum from experiment, and the depth of maximum does not vary according to the elongation rate theorem, then the composition must be changing (or the physics which governs shower development must be changing, thereby invalidating this form of the theorem). This analysis assumes that the energy and depth of maximum of each shower in the data sample is well known, which of course may not be true.

§ Once again, showers initiated by heavy nuclei develop faster than those initiated by protons. Simulations were carried out to determine whether the observed average development curves were more like those of iron or protons.

nucleus of an atom in the atmosphere to create a large number of secondary particles. These secondaries propagate through the atmosphere, interacting with other air nuclei or decaying and creating still more secondaries. This process continues until the original energy of the primary is shared between so many particles that none of them has enough energy to create more secondaries in subsequent interactions. The secondaries then just lose energy through ionization while traveling through the air and into the ground. This phenomenon is known as an air shower. When the primary has enough energy (generally defined as greater than 10^{17} eV) to create so many secondaries that the shower covers an extensive area when it hits the ground, it is called an extensive air shower or EAS. In addition to creating particles as it traverses the atmosphere, an air shower also emits light of various wavelengths via various processes. A shower initiated by a primary with energy between 10^{17} and 10^{20} eV, travelling vertically down through the atmosphere, typically begins with the primary interacting about 20 km above sea level. The shower attains its maximum development of 10^8 to 10^{12} particles at an altitude of about 2 to 0 km above sea level. Fluctuations in development, however, can change this behavior radically from one shower to the next.

2.2.1 Shower Components

An air shower can be divided into three components; the hadronic core, the muons, and the electromagnetic component. The hadronic core consists of secondary hadrons created in the nuclear interactions, namely the baryons (protons, neutrons, lambdas, etc.)

and the mesons (pions, kaons, etc.). Essentially all of the baryons and most of the mesons interact with air nuclei, creating more hadrons. After the first generation the hadrons give rise to, and lose energy to, the other two components. The hadronic core is quite closely packed, usually only about one meter thick and ten to thirty meters in diameter by the time it hits the ground.

Some of the charged pions and essentially all of the neutral ones decay before interacting to give rise to the other shower components. The charged pions give rise to the muons via the decay $\pi^{\pm} \rightarrow \mu^{\pm} + \nu$. Most of the muons hit and penetrate the earth, due to their long lifetime and small cross section for nuclear interactions. The spatial distribution of the muons in a shower at the ground is typically on the order of 500 meters radius and a couple of meters thick. The number density of muons in this disk varies exponentially with distance from the core. For showers with primary energy above 10^{16} eV, the muons are approximately as numerous as the hadrons in that shower, on the average.³⁰

The neutral pions, which have an extremely short lifetime (10^{-16} sec for the most probable decay, to two γ 's), give rise to the electromagnetic component of the shower. These γ 's convert to electron-positron pairs in the strong electric field near an air nucleus. The electrons and positrons (or just electrons for short), in addition to ionizing air molecules, can create more γ 's by brehmstrahlung, which in turn can convert to more electron-positron pairs. The electrons (the lightest charged particles) are copiously produced, being about one hundred times as numerous as the muons and

and hadrons of the other shower components (also note that the pions, which give rise to the electrons and muons, are the lightest and therefore most copiously produced hadrons in the shower core). At maximum development, the electrons typically cover an area of one to two hundred meters radius, with their density dropping exponentially with increasing distance from the core.

2.2.2 Light Output

As a shower traverses the atmosphere it emits light, mostly in the near ultraviolet. The two main processes for producing this light are Cherenkov radiation and atmospheric fluorescence (or scintillation).

2.2.2.1 Cherenkov radiation. When a charged particle traveling through a dielectric medium (like air or water) travels faster than the local speed of light (light travels slower in a dielectric than in a vacuum), it emits Cherenkov radiation at an angle relative to its direction of motion. Specifically, in a dielectric with an index of refraction n , the local speed of light is c/n (where c =speed of light in a vacuum), and the cosine of the angle between the emitted light and the direction the emitting particle travels is $\cos(\theta)=c/v \cdot n$, where v is the speed of the emitting particle. For air shower particles in the atmosphere (where v is essentially equal to c) this angle is about one degree. Since the rms scattering angle of the shower electrons relative to the axis of the shower is much larger than that (about ten to fifteen degrees³²), the angular distribution of Cherenkov light coming from an air shower is essentially that of its electrons.³¹ A shower particle

travelling with speed c at sea level will emit approximately 500 Cherenkov photons per meter of trajectory in the wavelength interval between 650 and 275 nm, with the numbers emitted in the higher atmosphere decreasing approximately as the air density decreases. Typically, a shower with energy above 10^{17} eV produces 10^{12} or more Cherenkov photons inside an area about one kilometer in radius, with the number density of photons dropping exponentially with increasing distance.³²

2.2.2.2 Scintillation light. The scintillation light is emitted by air molecules (mostly N_2) that have been excited by the passage of the shower particles. The excited molecules can de-excite either by emission of light, or through collisions with other molecules. The angular distribution of this light is isotropic and the production efficiency of the light is almost independent of altitude. This is because while there are more molecules to be excited per meter of track length lower in the atmosphere, there is also a greater chance of collisional de-excitation. These two effects combine to lead to a fluorescence efficiency of about four photons per shower particle per meter of trajectory. The actual number only varies by about twenty percent over the range of pressures encountered by an air shower in the atmosphere.^{33,34}

2.3 Traditional Techniques for Detecting UHCR's

Traditional experimental detection schemes fall into two categories: particle detectors and atmospheric Cherenkov detectors.

2.3.1 Particle Detectors

Particle detectors are devices that require the shower particles physically to hit the detector. Due to the large number of particles in a typical EAS (extensive air shower) when it hits the ground, it is not necessary to actually instrument the entire area that is covered by the shower impact. Instead, one usually scatters detectors about an area, separated by ten to one hundred meters, and interpolates among the numbers of particles counted by each detector to calculate a fairly complete shower density profile (depending on the fineness of the sampling).

2.3.1.1 Electron detectors. In order to measure the number of charged particles in a shower when it hits the ground (most of which will be electrons), one usually uses scintillation counters. Relatively cheap and rugged, such detectors usually take the form of sheets of plastic or vats of liquid scintillator about a square meter in area, with photomultiplier tubes (PMT's) converting the light output from the scintillator into electrical signals. Arrays of these detectors are often a couple of square kilometers in area (for example, Haverah Park or Volcano Ranch²⁷). The information obtained from these detectors (the number of particles that hit each sheet and the time they hit) can be used to determine the direction the shower was traveling (an inclined shower will arrive at some sheets sooner than others) and the total number of shower particles at ground level (by interpolation). This number of particles can be used to estimate the energy of the primary particle. However, due to inaccuracies in determining the stage of shower development at

the ground (the so-called "age" parameter), and due to fluctuations in individual shower development, these estimates may be inaccurate. Scintillation counters have been used in all of the big cosmic ray arrays.^{21,27}

Another detector for measuring the number of charged particles in a shower is the deep water Cherenkov tank (DWCT).²⁷ Used at Haverah Park, these detectors depend on the fact that water, due to its high index of refraction, is a rather efficient Cherenkov radiator. The angular distribution of the light can be quite wide, being forty degrees for particles traveling at the speed of light. So a deep vat of water, containing a few PMT's (photomultiplier tubes) to convert the Cherenkov light pulses to electrical signals can make an efficient and cheap particle detector. Care must be taken, however, to keep the water very clean or transmission of the Cherenkov light through the tank will suffer.

By use of modern extruded aluminum tubes and integrated circuits, it has become possible to build large inexpensive proportional chambers. These detectors consist of a long conducting tube with a tungsten or stainless steel wire (used for their high resistivity) running down the middle. The wire is held at a high potential relative to the tube, and a special gas (usually argon with a small admixture of methane, so-called P-10 gas) is circulated through the tube. When a charged particle passes through the gas, it creates ion pairs. The liberated electrons from these pairs are accelerated toward the wire by the potential, knocking other electrons out of atoms along the way. This cascade of electrons is

gathered by the wire. When properly operating, the charge collected by the wire is directly proportional to the number of ion pairs created by the particle passing through the gas. If the signal is taken off both ends of the struck wire, the relative size of the pulses can be used to locate where the ions were gathered along the wire. This feature is used to reconstruct the trajectory of individual hadrons in the shower core and study their interactions with matter surrounding the detector. Of late, advances in materials and electronics have brought the cost of proportional chambers below that of similar sized scintillators, and plans exist to build large arrays of such chambers to detect shower electrons.³⁵

2.3.1.2 Muon detectors. Muon detectors are essentially electron detectors shielded by concrete or earth (or other dense material) to absorb the electrons (electrons are highly ionizing and quickly lose their energy in solid matter). Due to the fact that the relatively heavy muons are not efficient Cherenkov radiators (the critical energy for emission of Cherenkov photons in water is 300 Mev for muons versus 1.5 MeV for electrons), DWCT's are not very efficient at counting low energy muons. However, for high energy muons at distances greater than about 500 meters from the shower core (where about the only particles left to be counted are muons) DWCT's do a quite satisfactory job. In fact, the primary energy estimator used for the Haverah Park array is the signal in a DWCT located 600 meters from the shower core (the so-called " $\rho(600)$ " parameter). This number is usually found by interpolation.

Scintillators are also used for counting muons. By burying the

detector deeper in the earth, one can pick off only the higher energy muons, the lower energy ones being stopped in the overburden. These higher energy muons tend to originate early in the shower, where there is more energy available per particle. However, one usually requires two or more muons in one's detector for a trigger to prevent the detector from triggering on natural radioactivity from the surrounding rock. Requiring this higher number density of muons means that by burying one's detector deeper, one triggers on higher energy showers.

2.3.1.3 Hadron detectors. The hadronic core of a shower can be measured in a variety of ways (proportional chambers, nuclear emulsions, etc.). Hadrons are separated from shower electrons by their greater penetrating power and from muons by their much greater likelihood of undergoing nuclear interactions. Unfortunately, the small area of the core (approximately one to one hundred square meters), the low rate at which high energy cosmic ray showers arrive (about .04 per square meter per year from all directions for all energies above 10^{17} eV), and the small area of these detectors (typically several square meters) make measuring properties of hadrons a rather futile undertaking at the energies addressed by this experiment. At lower energies the rate is much more reasonable, and in the days before high energy particle accelerators much useful physics was done using air shower hadrons.

2.3.2 Atmospheric Cherenkov Detectors

Another method of detecting air showers is to use optical sensors to detect the Cherenkov light emitted by the shower in pas-

sing through the atmosphere. In its simplest form, a Cherenkov detector consists of a PMT exposed to the sky with some fast electronics connected to the output (the Cherenkov light pulse from a shower varies on a time scale of tens of nanoseconds). Since Cherenkov light is continuously emitted during the lifetime of the shower, the shape of the light pulse contains information about shower development. The Cherenkov pulse width, rise time and pulse height are usually measured and compared with the results of simulation.²⁷ Arrays of Cherenkov detectors can be operated in the same way as particle detectors to determine the trajectory of the showers. Further refinements to the bare PMT detector usually involve placing the PMT's at the focus of a mirror to collimate and increase the collection area of each PMT. Note that the shower must hit near (within a kilometer or so) the detector in order for this technique to work. This technique is used to some extent by many of the large arrays, and played an integral part in the experiments at Yakutsk and Sydney.^{21,26}

2.3.3 Present Detectors and Their Limitations

There are several arrays scattered across the world that use a mixture of the above techniques to measure properties of air showers with energies above 2×10^{17} eV. The longest running experiments (and the integral spectra they measure) are: Haverah Park, England (spectral index 2.05 ± 0.02 , based on 11,000 events),³⁶ and Yakutsk, USSR (spectral index $2.05 \pm ?$, data being reanalyzed).²¹ Another experiment at Sydney, Australia has not yet presented final data, but preliminary results ($\gamma = 1.96 \pm 0.02$) are similar to those of the other groups.³⁷

Note that all the above techniques suffer from two limitations. First, the shower must physically hit the detector, or in the case of Cherenkov detectors, hit within a kilometer. While the sampling and interpolation techniques mentioned earlier allow one to instrument only a fraction (about one percent to ten percent) of the active area of the detector, one is still restricted to areas no larger than a couple of square kilometers. Since the integrated rate of showers initiated by primaries with energies in excess of 10^{19} eV is only about 0.4 per square kilometer per year, the rate of detection of high energy showers is low. Second, these techniques (except for the Cherenkov technique) sample the shower at only one point along its trajectory, namely at ground level. Atmospheric Cherenkov detectors can theoretically provide information about the shower development, but in practice only a very rudimentary knowledge of shower development can be obtained (the Cherenkov photons produced in different parts of the shower arrive at the detector within a time interval of ten to thirty nanoseconds, making extraction of actual shower profiles impossible). Nevertheless, Thornton and Clay²⁶ were able to use this technique to measure the depth of maximum development of showers in the energy range 10^{15} to 10^{17} eV, and thereby to infer a change in composition. The Chacaltaya experiment,²⁸ by looking at showers arriving at different zenith angles but at the same rates (and assuming that this meant that those showers were at the same energy) was able to determine the average development of those parts of the showers that had penetrated more than 550 gm/cm^2 deep in the atmosphere. However, these were average

development curves, and simulations³⁰ suggest that deviations from average development can be quite large. What was needed was a technique that both increased the rate at which high energy showers were detected (especially above 10^{19} eV, where the primaries are expected to travel nearly in straight lines from their sources), and provided information on shower development on a shower-by-shower basis to give information on the composition of the primaries and on particle interactions at ultra-high energies. A technique that offers some promise in solving some of the above problems is detection of scintillation light from air showers, by a detector like the Utah Fly's Eye.

CHAPTER 3

THE FLY'S EYE

3.1 Theory of Operation

As an air shower traverses the atmosphere, it excites air molecules, causing them to emit scintillation light. The decay time for this excitation is sufficiently short (about 50 nsec or less,³⁴ the time required for the shower front to travel about 15 meters) that the light is emitted very close to the shower front. What one would see, if one were standing a couple of kilometers away, would be a compact light source radiating in the blue and near ultraviolet with about the intensity of a five watt bulb, traveling across the sky at the speed of light. This is the phenomenon the Fly's Eye was designed to detect.

3.1.1 Gathering of Light

The light emitted by the air shower is gathered by concave spherical mirrors. These mirrors focus the the light onto PMT's, which convert the light signal into an electrical signal, specifically a certain amount of charge. The time at which the signal arrives at the detector and the integral of the signal are stored on computer for each PMT that detected the event. The mirrors and tubes are arranged such that each PMT looks at a different part of the sky, like one of the elements of the compound eye of a fly, hence the name of the detector. The entire night sky is covered by

880 PMT's.

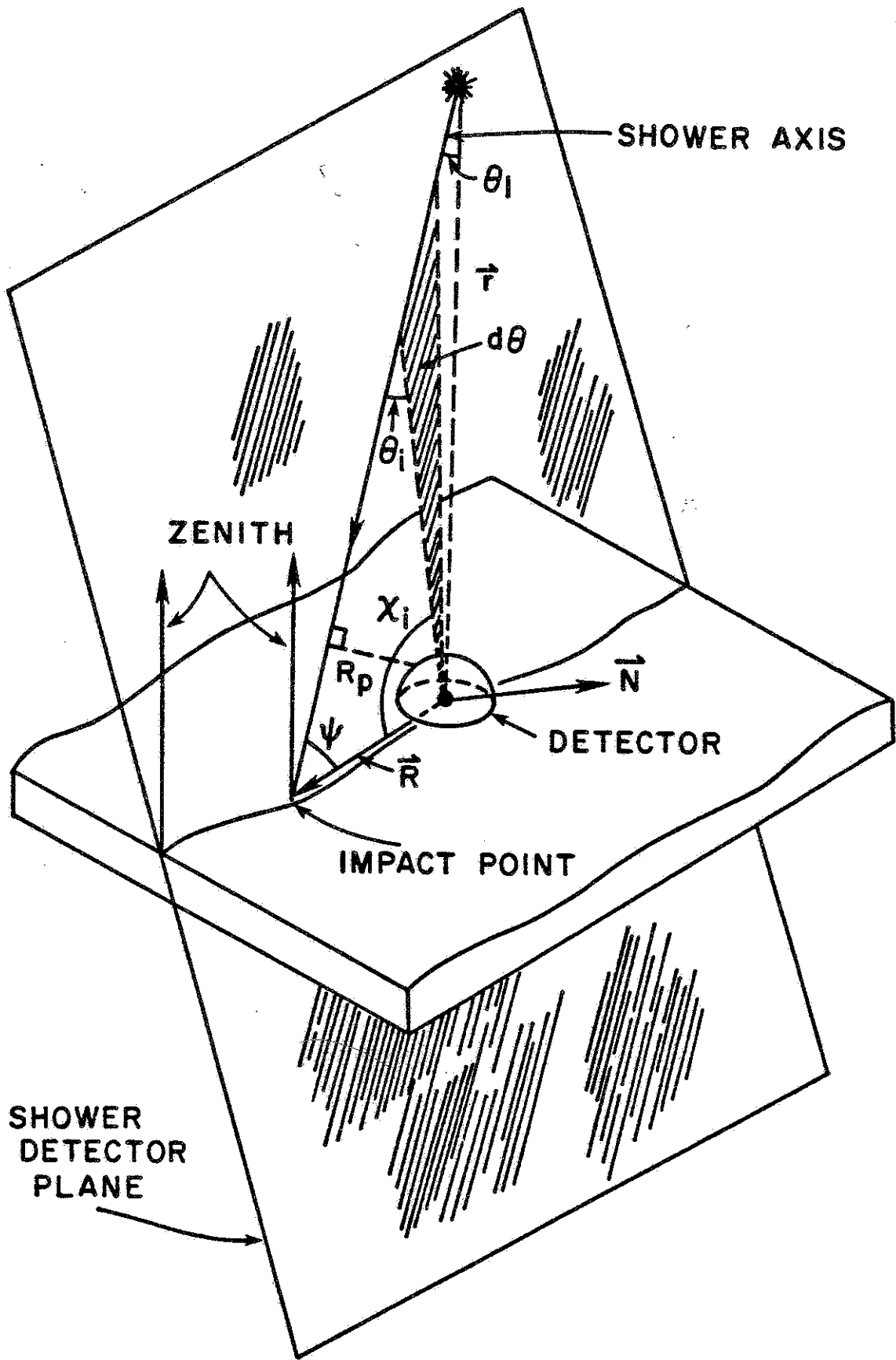
3.1.2 Geometrical Reconstruction

Determining the trajectory of an air shower requires the specification of four parameters, two to determine the orientation of the plane containing the shower and the detector (the "shower-detector" plane) and two to specify the geometry of the shower "line" in that plane. Given the times at which each PMT received a signal, and the direction in which each of those PMT's looks, these parameters can be determined. The observation angle of each PMT defines the shower-detector plane and the time between the arrival of the light pulse in adjacent PMT's determines the line in that plane. The further away the shower is from the detector, the longer the times between adjacent PMT pulses. If the shower is approaching the detector, the time between adjacent pulses will decrease, while for receding showers the time between adjacent pulses will increase.

To be specific, suppose a shower trajectory appears as in Figure 2. The information gathered by the Fly's Eye in such an event is: the tubes that see the event (i), the relative times at which the light pulses arrived at the detector (T_i), and the integrated signal (or charge) from each of those PMT's (which to a first approximation is not needed for the geometrical reconstruction). Also known is the observation direction of each PMT (\underline{D}_i). The event is reconstructed as follows:

The shower-detector plane, defined by its normal vector \underline{N} , is found by searching for \underline{N} such that $\sum \underline{N} \cdot \underline{D}_i$ is a minimum. Hav-

FIGURE 2
Reconstruction Geometry



ing found the shower-detector plane (defined by the coordinates of the normal vector \underline{N} ; θ_n and ϕ_n) we next need to determine the parameters R_p and ψ (as defined in Figure 2) which define the orientation of the shower trajectory in that plane. They are found by fitting the times, T_i , to the equations:

$$T_i = T_0 + (R_p/c) \cot(\psi + \chi_i) \quad (1)$$

where the χ_i can be determined from the \underline{D}_i and \underline{N} .[†] Equation (1) is derived as follows:

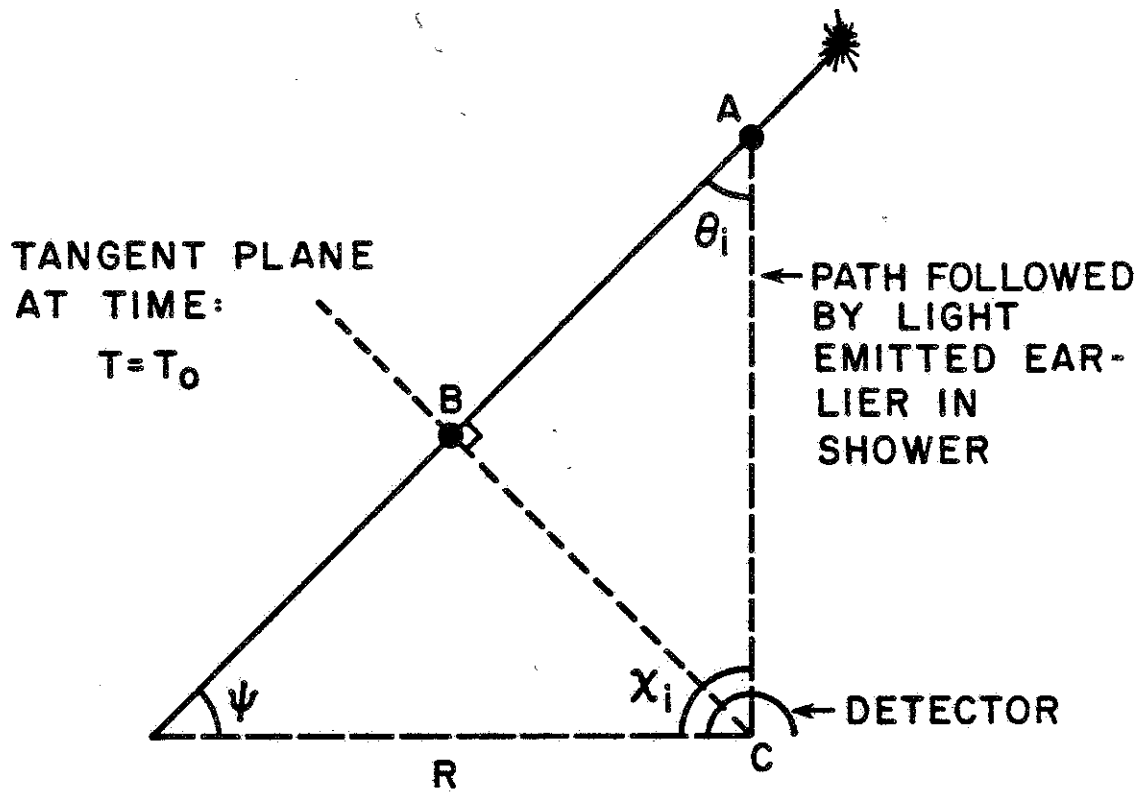
Consider a plane (called the tangent plane,³³ see Figure 3) perpendicular to the shower track, parallel to the shower front and moving with it. Obviously, the light signals from earlier in the shower will reach the detector after the tangent plane has swept past, but by how much? From Figure 3, we see this will be $T_i - T_0 = (AC - AB)/c$. From consideration of the triangle ABC, we see this can be written:

$$\begin{aligned} T_i - T_0 &= (1/c)(R_p/\sin(\theta_i) - R_p/\tan(\theta_i)) \\ &= (R_p/c)\tan(\theta_i/2) \end{aligned} \quad (2)$$

However, $\theta_i = \pi - \psi - \chi_i$. Making this substitution in equation (2) gives us equation (1). If n tubes see the event, this gives us n equations in three unknowns; T_0 , R_p , and ψ . By use of a non-linear least squares fitting routine, we can then determine the final two parameters needed to determine the shower trajectory.

† To find the χ_i , first find the unit vector \underline{R} that points along the ground from the detector toward the shower impact point. Then χ_i is defined by $\underline{D}_i \cdot \underline{R} = \cos(\chi_i)$. The conditions $\underline{N} \cdot \underline{R} = 0$ and $R_z = 0$ give two choices for \underline{R} . The correct choice is found by determining for which one $\underline{D}_i \cdot \underline{R}$ corresponds to a larger angle than $\underline{D}_n \cdot \underline{R}$, where \underline{D}_n is the last tube to see an event.

FIGURE 3
Tangent Plane Relative
to Detector



3.1.3 Size Analysis

Knowing the trajectory of the shower, we can use the integrated signals to calculate the numbers of charged particles at various points along the shower track. From the calibration of the electronics, we can determine the number of photons gathered at the PMT face from the size of the integrated pulse. This number of photons, along with the knowledge of the trajectory, allows us to determine the number of photons that must have been emitted by that portion of the shower. As mentioned in Chapter 2, the number of scintillation light photons emitted per shower particle per meter of air is well known. This allows us to calculate the average number of charged particles in the field of view of each PMT that sees the shower. Knowing the numbers of charged particles at various points along the trajectory of a shower, we can compare these numbers with shower profiles generated by simulation to get, among other things, the energy of the shower.

3.2 The Detector

3.2.1 Physical Layout

The Fly's Eye detector consists of 67 sixty-two inch diameter front aluminized mirrors, with either 12 or 14 PMT's at the focus of each mirror (as shown in Figures 4-8). The detector is arranged about the top of Little Granite mountain in the Dugway Army Proving Grounds, located in the Basin and Range physiographic province of the western United States. From the top of this 500 foot tall hill, we have an unobstructed 360° view of the sky. The mirrors and PMT's are housed in metal "cans" (Figures 4 and 5) with

FIGURE 4

Aerial View of Detector

Top photo: Aerial view of Little Granite Mountain, Dugway Army Proving Grounds, Utah.

Bottom photo: Overhead view of detector showing cans, cable troughs, electronics trailer and living quarters (center of picture), and Army radio station (upper left).

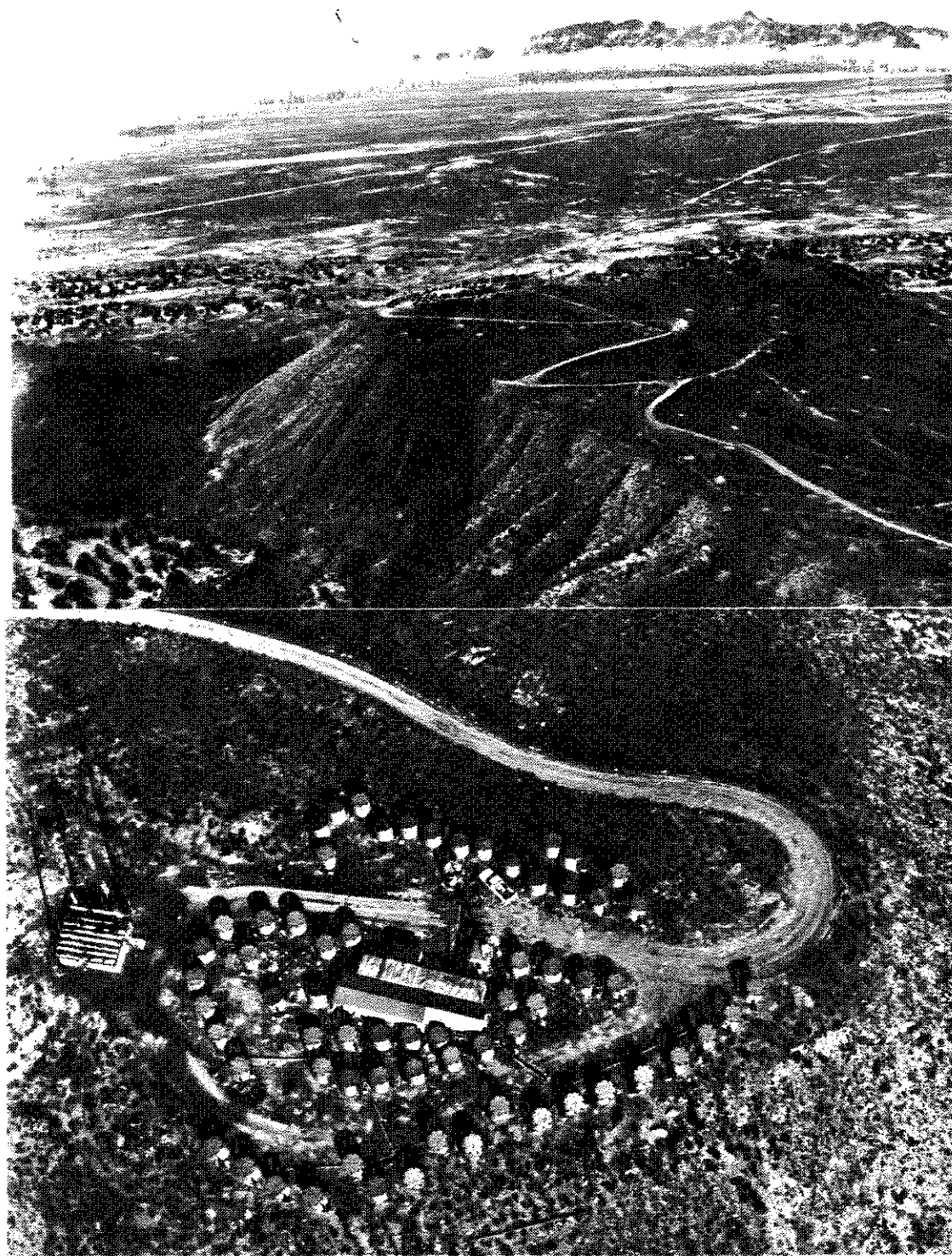


FIGURE 5

Inside View of Mirror Housing

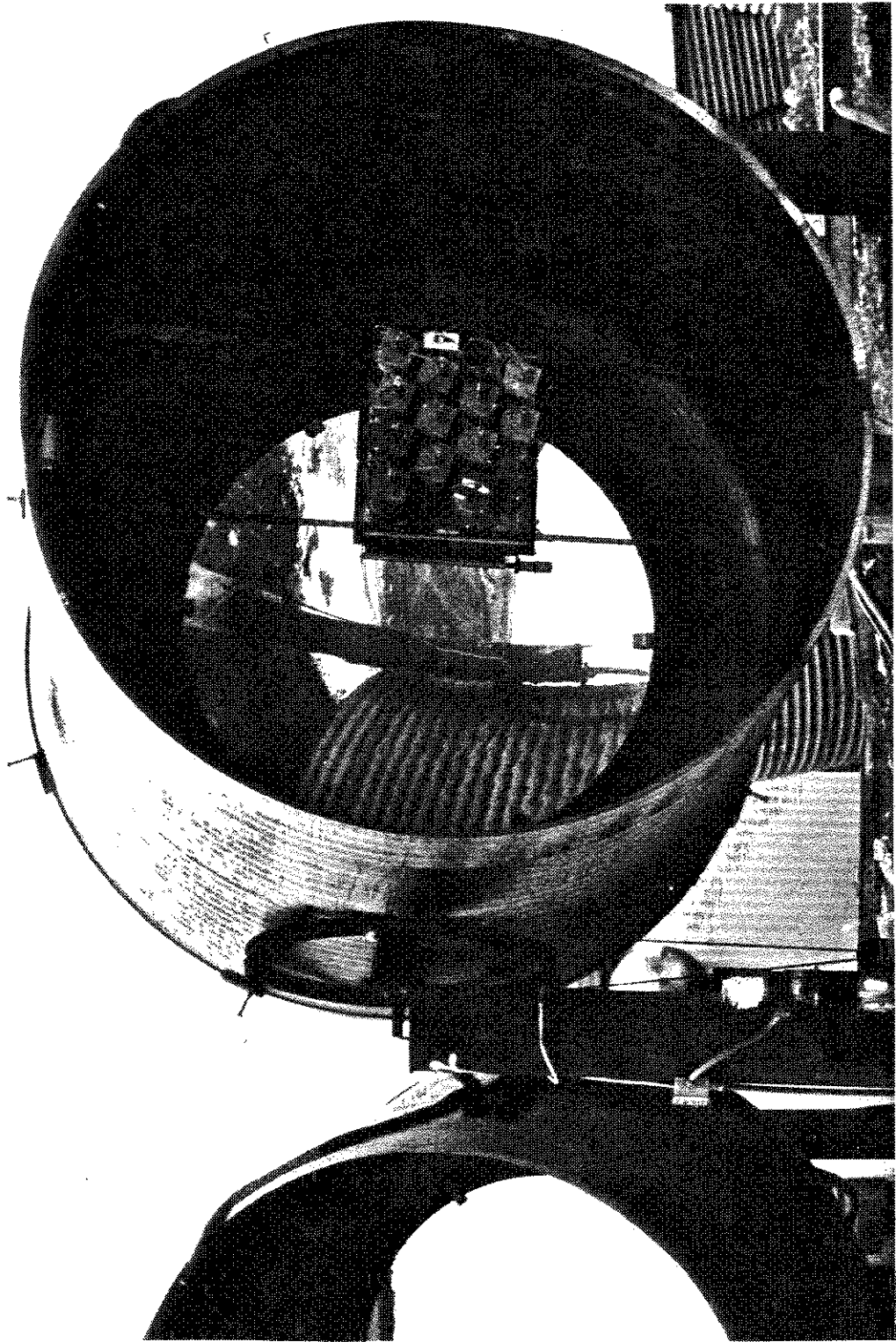


FIGURE 6

Inside Trailer-Ommatidial Racks

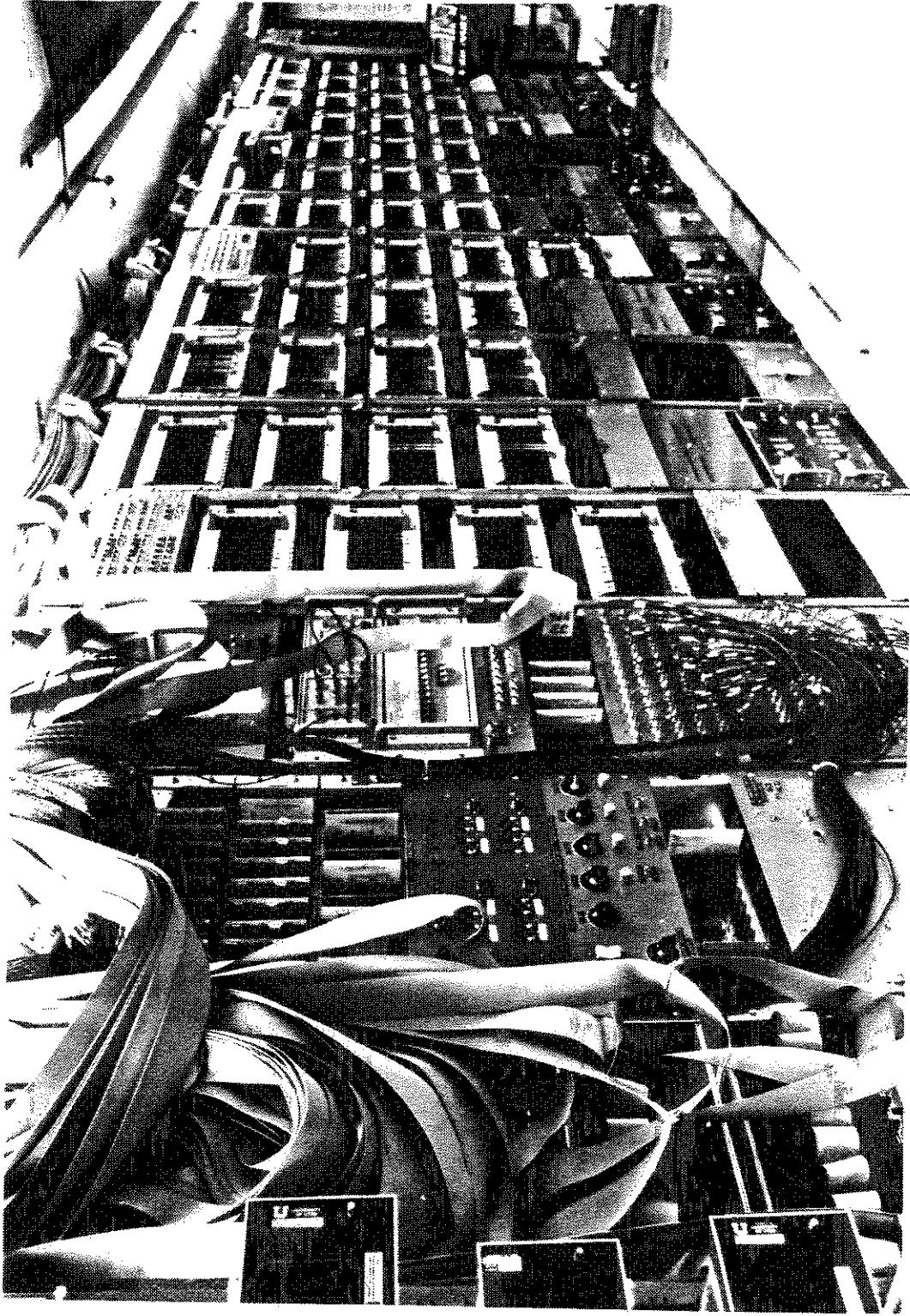


FIGURE 7

Inside Trailer-HV Racks and
Back of Ommatidial Racks

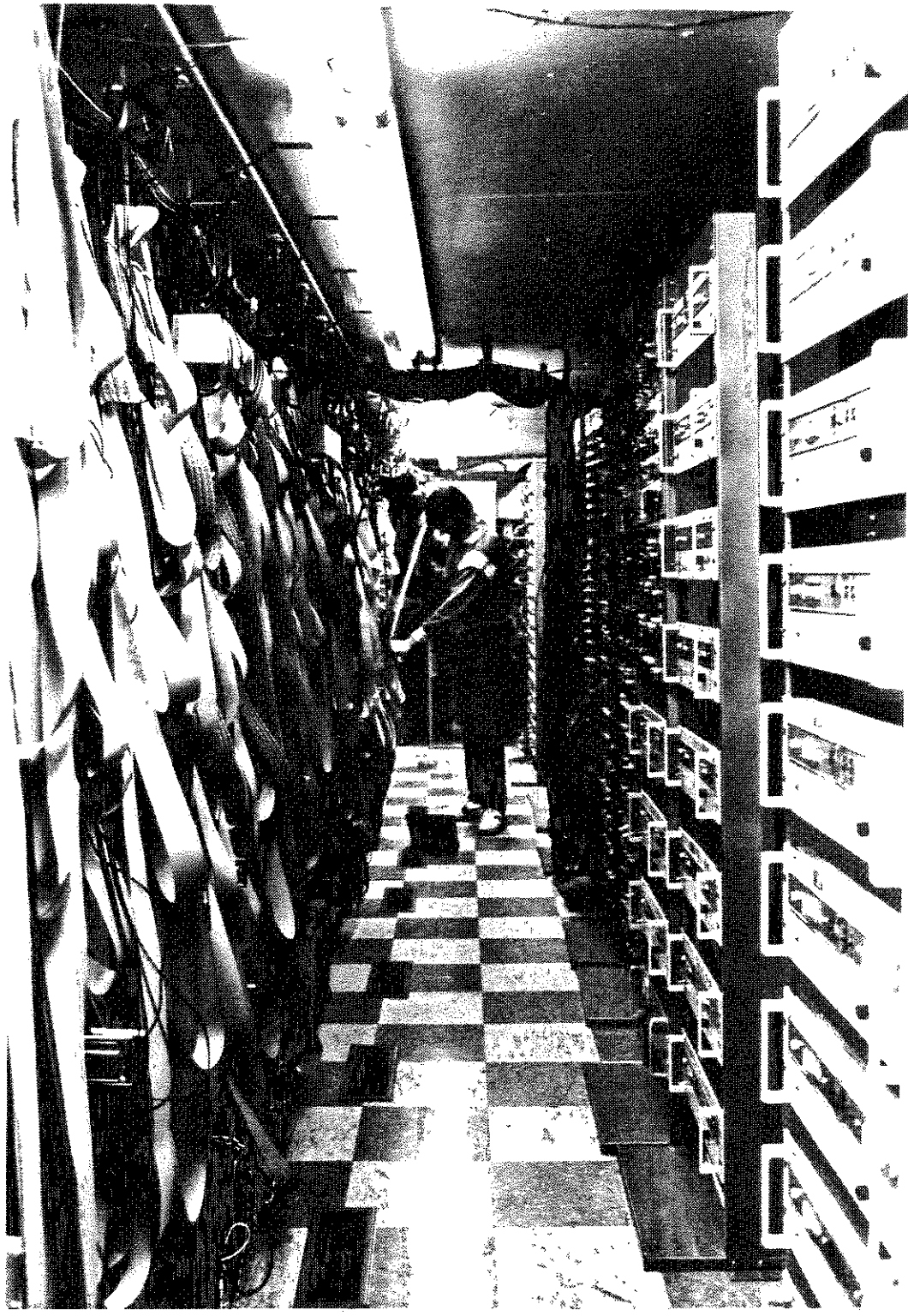
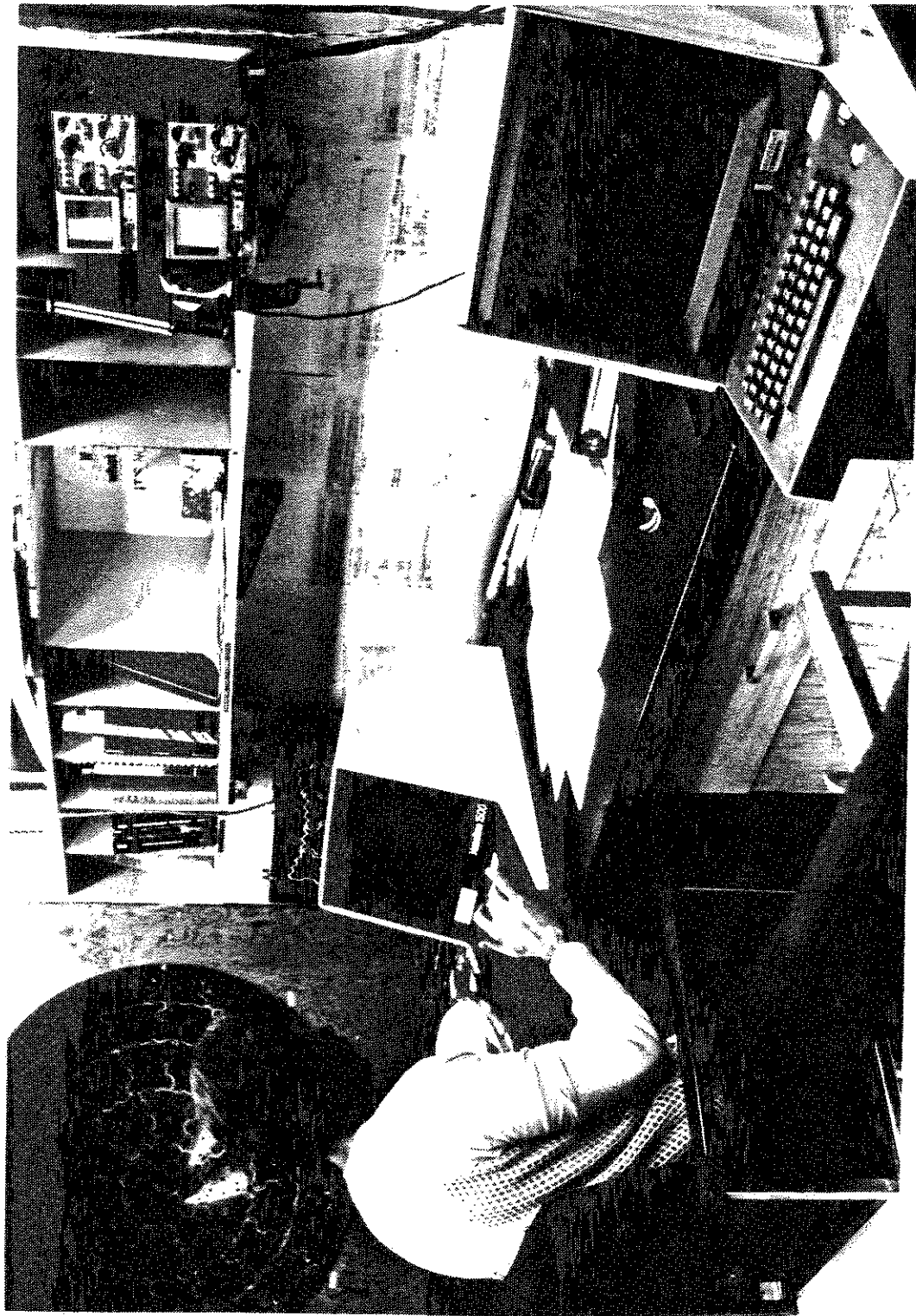


FIGURE 8

Inside Trailer-Operator's Console
and Event Display



one end open, that can be pivoted up to see the night sky, or down to protect the mirrors and PMT's from the sun and weather. In addition, trailers containing electronics, a PDP 11/34 computer used to control the experiment, and rudimentary living quarters, are also situated at the top of the hill (Figures 6-8).

3.2.2 System Overview

3.2.2.1 Data path. When the light pulse from an air shower hits the PMT face, each photon in the pulse on the average gives rise to 10^4 electrons at the PMT anode. This charge pulse is routed through a transconductance amplifier (with an effective feedback resistance of 65.6 k Ω) located at the PMT base, and is then cabled into the electronics area. Inside, this signal goes to an ommatidial[†] board where it is split; one portion being delayed and then sent to a gated integrator, the other portion going to a discriminator that provides the gate. If the pulse is high enough to trigger the discriminator, the signal is integrated and held, pending its being digitized and read (if a hardware trigger is formed) or cleared (if it is not).

3.2.2.2 Triggering. In order to separate the useful cosmic ray events from noise due to starlight, airplanes, and the more frequent low energy showers that approach the detector head-on (giving us a blast of Cherenkov light and no timing information from which to reconstruct its geometry) we impose a hardware coincidence re-

[†] This term comes from "ommatidium," a nerve junction in a fly that preprocesses the signal that comes from each element of its compound eye.

quirement and a software filter before recording an event. The hardware coincidence at the time this data was taken required that at least two PMT's in each of three different mirrors fire within a certain time, but that the signals from each mirror had to be separated by a certain minimum time. If these requirements were met, a computer read in the integrated signal from each PMT that saw the event, and the times at which they fired. A few quick software cuts were made (based on the number of tubes in the event and the total time elapsed from first tube to the last) and if the event passed the cuts, it was recorded and stored for later analysis.

3.2.3 Software

The software that is used to run the detector can be divided into sets of routines that perform three functions; data acquisition, calibration, and diagnostics. All that need be said of the diagnostics package is that it consists of a series of routines that exercise all of the electronics of the Fly's Eye. Run each night prior to turning the detector on, these routines will usually pinpoint electronics failures to a single circuit board, which can then be immediately replaced by a working spare.

3.2.3.1 Data acquisition. The data acquisition system (known as "FLY") is a series of routines that controls the detector operation. In addition to reading in and storing what appear to be good events, FLY also monitors system integrity, alerting the operator of possible problems and setting the trigger thresholds on the ommatidial boards to keep the Eye operating at peak sensitivity given a varying

source of noise (i.e., background light). FLY also performs the software filtering.

3.2.3.2 Calibration. The calibration of the Fly's Eye is performed in several steps. The operating voltages of the PMT's are set by using radioactive sources mounted on scintillator crystals as standard light sources (special holders allow us to do this with the PMT's in place in the detector). The PMT's are then monitored by use of a flash tube apparatus mounted in the cans. These flash tubes are also used to monitor the reflectivity of the mirrors. The gains of the data path electronics (PMT base amplifiers and ommatidial board integrators) are calibrated with a programmable pulser at the lab and monitored by a programmable pulser on site. Diagnostic software flags the gains and pedestals of all analog electronics if they fall outside certain limits. Typically, gains are maintained to within $\pm 4\%$ and all pedestals are kept positive and their values are recorded on a nightly basis for subsequent data reduction. Finally, a xenon flasher was taken to various sites around the detector, and fired into the sky. The scattered light from the beam triggered the Fly's Eye and the subsequent "fake" events, whose trajectories were known, were used to calibrate the software used in the geometrical reconstruction.

CHAPTER 4

DATA ANALYSIS

Data analysis was performed by a four-step process, the first two steps being common to any experiment using Fly's Eye data, the last two being specific to this experiment.

4.1 Scanning

A routine called SCAN is used to visually discriminate the useful events in the raw data files written by FLY from those noise events that make it past the software filters. Run in an interactive mode, SCAN simply displays which PMT's saw a given event. An operator then tells the routine whether to reject an event, or to write it into a special file for later analysis. The acceptance criteria are quite loose, requiring only a recognizable track that subtends at least 30° of arc (about six tubes long), with the tubes in the track for the most part in the correct time order.

4.2 Geometrical Reconstruction

GEO is the routine that reconstructs the geometry of the scanned events. To do so, it essentially uses the program outlined in section 3.1.2. In reconstructing an event, we usually made several passes at the data, using the results of the previous pass to make various geometrical corrections. Before the first pass,

the latch times, T_i , are corrected for cable delays (some PMT's have longer cable runs to the electronics than others). After the first pass, the pulse width and trajectory information from that pass were used to correct the pulse arrival times (T_i) for time slewing (which delays the latched time for low amplitude pulses) and the finite size of the detector (the detector is spread out over an area about 100 by 200 meters). At least two, and usually more passes were made at each event. When, in comparing the results between one pass and the next, the parameter R_p changed by less than its fitting uncertainty, one final pass was made. The values of the parameters determined by the last pass were chosen to define the trajectory (in this case, we were only interested in the R_p distribution of the events). After an event was reconstructed, the operator decided whether to reject the event or to write it onto a special file for later analysis. This decision was made strictly on the basis of geometrical cuts such as the size of R_p and the angle subtended by the track in the sky.

4.3 Binning of Reconstructed Events

RPGE0 is the routine that was used to take the events reconstructed by GEO, and bin them in impact parameter (R_p). It can also print out histograms and scatterplots of the uncertainties of the reconstruction variables for use in later analysis. The size of the R_p bins was chosen to be $R_p \pm 7.8\%$ or about equal to the average fitting uncertainty of the reconstructed events. Several runs of RPGE0 had to be made to determine what was the correct bin size and to gather the distributions of uncertainty used to

calculate the "slopovert" of events from one bin into adjacent bins. This information was used in simulating the detector response.

4.4 Simulation of Detector Response

SPECSM is the routine that simulates the response of the Fly's Eye. It takes the aperture of the detector, splits it into about 20,000 bins, determines a trajectory whose geometry is representative of a given bin, and calculates the minimum energy necessary for an air shower with that trajectory to trigger the detector. Given this energy, we can determine the rate at which such showers will trigger the detector. By summing the rates in these bins in R_p and multiplying the summed rates by the time that the detector was on, we obtained a distribution that can be compared with the experimental distribution binned by RPGE0. In order to get agreement between these distributions, we varied the parameters of the simulation (principally the spectral index and normalization used to calculate the rates) until the simulated distributions and the experimental distributions agreed.

4.4.1 Simulation Geometry

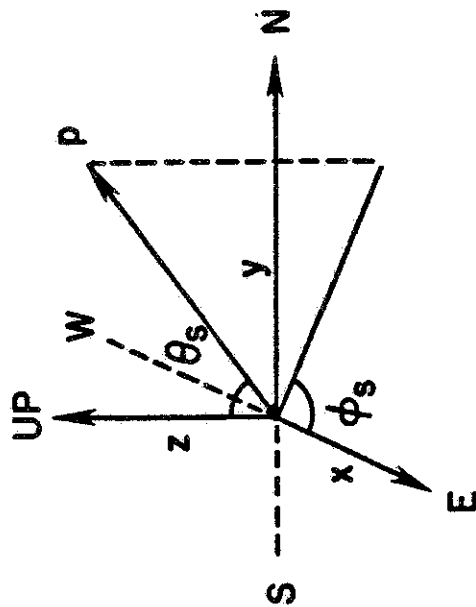
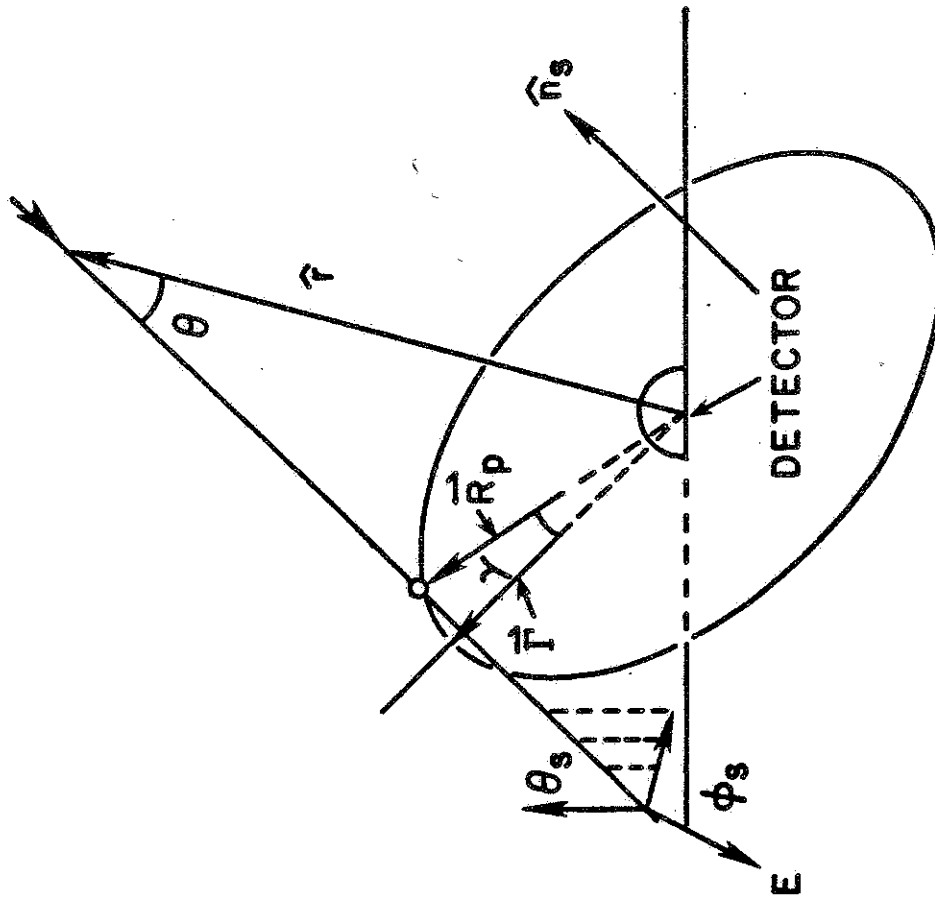
The variables used in the reconstruction of events were chosen with ease of calculation in mind. However, for purposes of simulation those variables are rather clumsy, so another set of variables was chosen (see Figure 9).

As in the reconstruction geometry, four parameters are used to specify the shower trajectory relative to the detector: R_p , θ_s , ϕ_s , and γ . Using this geometry, the total aperture was broken

FIGURE 9

Simulation Geometry

This figure shows the simulation variables R_p , γ , θ_s , and ϕ_s . Also shown is the way the angles θ_s and ϕ_s are defined relative to the local directions and the shower-detector normal plane (analogous to the "tangent plane at $T=T_0$ " shown in Figure 3). The vector $\underline{\Gamma}$ (from which the angle γ is measured) is defined as the vector in the shower-detector normal plane with the largest z -component. Together these parameters give the direction of the shower (θ_s and ϕ_s), the impact parameter of the shower (R_p) and the location of the shower relative to the detector (γ).



into bins in the following manner: 13 R_p bins ($R_p \pm 7.8\%$ from 1 to 7 km), 15 bins in γ , and 100 bins of equal angular area in $\theta_S - \phi_S$, making 19500 bins in all. These bin sizes were chosen after several runs of the simulation routine showed that using smaller bin sizes did not improve (or even change) the results.

4.4.2 Simulation Algorithm

The following approximations were used in simulating detector response:

- i) The earth is flat (this approximation is good to better than 1% up to 50 km away for all geometries of interest).
- ii) The density of the atmosphere is an exponential function of height.
- iii) The incoming primaries are all protons that undergo their first interaction 60 gm/cm² deep in the atmosphere.
- iv) The subsequent longitudinal development of the shower is that of an "average" shower, as defined by the Gaisser-Hillas parameterization.³⁸

While increasing accuracy by dropping approximations i and ii would probably have no observable effect on the spectrum determination given the current accuracy of reconstruction of showers, dropping iii and iv might, particularly if one is investigating the finer details of the spectrum. However, we consider these to be reasonable approximations for a first attempt at a spectral measurement for the following reasons: First, as mentioned in Chapter 2, the preponderance of evidence suggests a mainly proton composition above 10^{17} eV. Since the interaction length for a high energy

proton in air is about 60 gm/cm^2 , this may be taken as an average depth of first interaction. Second, an average shower development would give an average light output to the detector. Since one would expect the response of the Fly's Eye to a large number of "average" showers to be about the same as to the same number of real showers, and since there is little virtue in making one's calculations any more complex than necessary, these approximations were chosen.

The algorithm used to simulate the detector's response (specifically the rate at which showers would trigger the Fly's Eye, and their distribution in R_p) is as follows: First, pick a trajectory (i.e., an aperture bin) and determine which PMT's would see it. If this collection of tubes is capable of triggering the detector and passing the same geometrical cuts as the real data, continue. If not, pick a new trajectory and start over. Next, determine individually for each PMT that sees the shower what is the minimum energy necessary for a shower with that trajectory to emit enough light to trigger that tube (actually to trigger the discriminator on the ommatidial board for that tube). This is done by simulating a shower (and its attendant Cherenkov beam) down to the field of view of the tube of interest, then determining the signal in that PMT due to scintillation light, direct Cherenkov light and scattered Cherenkov light (including both Rayleigh and aerosol scattering), from that portion of the shower.[†] The energy

[†] The signals in the PMT's were calculated using light production routines written by J. Elbert, stemming from work that he, T. Gaisser, and others are doing on simulations of showers.

of the shower is adjusted up or down until the signal just barely triggers the PMT of interest. Once this tube trigger energy is known for each PMT that sees the shower, we take the six tubes with the lowest such energies (because six is the smallest number of tubes that can trigger the detector), and see if this collection of PMT's is capable of triggering the detector and passing the geometrical cuts. If they are not, we pick the seven lowest energy tubes and try again. If they are, the highest of this collection of tube trigger energies is considered to be the minimum energy necessary for a shower with this trajectory to trigger the detector. This energy, and the four parameters defining the trajectory, are then written in a special data file for later analysis. The program then moves on to the next bin.

Calculation of the simulated R_p distribution is performed by a routine called EBIN. This routine reads the data file written by SPECSM and uses the trigger energy for each bin to calculate $I(>E)$ for that bin (and therefore the rate at which showers fall in that bin). These rates are then summed over all angular variables to give a rate distribution in R_p . After multiplying the rates by the length of time the detector was on to give a number distribution, we compare these numbers with the actual distribution of showers as binned by RPGE0. The parameters A and γ (normalization and spectral index) are then varied until the simulated distribution matches the experimental distribution.

Specifically, we determined A and γ in the following manner: The number of events that will have trajectories in a given trajec-

tory bin will be $dN = I(>E) \cdot (dA\Omega) \cdot t$, where $dA\Omega$ is the size of the aperture bin, t is the time the detector was on, and E is the trigger energy for that bin. This can also be written :

$$dN = A \cdot t \cdot E^{-\gamma} \cdot (dA\Omega) \quad 1$$

Let $E^{-\gamma} \cdot (dA\Omega)$ be the "unnormalised" rate for an aperture bin. If we sum the unnormalised rates over all angular variables, we get the unnormalised rate distribution in R_p ; dR_i . If we then sum the dR_i , we get an overall unnormalised rate, R_u , which is directly proportional to N , the total number of events seen by the Fly's Eye. We can then set up the equality $N = F \cdot R_u$ to insure that the simulated distribution refers to the same number of events as the experimental distribution, then plot $F \cdot dR_i$ versus dN_i (the number of events in each R_p bin for the experimental distribution). Once we find a γ (and F) that gives good agreement between the two distributions, we note that $F = A \cdot t$. Knowing t (the on time for the detector), we can calculate A , the normalization.

CHAPTER 5

RESULTS

5.1 Raw Distribution

The final fits were performed on the distributions shown in Figures 10 and 11. Sample (a), shown in Figure 10, consists of 1137 events gathered in 800 hours of running between September 8, 1980 and October 5, 1981. The showers were required to have R_p greater than one kilometer and a track length which subtends an angle of 50° or greater. We found that Cherenkov light from showers with small initial viewing angles (θ_i) would trigger PMT's adjacent to the track (see Figures 12 and 13) complicating the geometrical reconstruction. To correct for this problem, we required longer track lengths for those showers. Essentially this meant that in determining whether or not a shower subtended 50° of arc, we did not use tubes with viewing angles less than 20° . Sample (b) (see Figure 13), a subset of sample (a), consists of 397 showers with track lengths greater than 70° , with no cut on initial viewing angles. This sample was used to determine the effects on the fit of more stringent geometrical cuts.

5.2 Simple Parametric Fit to Data

Before performing the simulation, we made a quick estimate of the spectral index. For this we fit the functional form:

$$dN = D \cdot R_p \gamma^{-2.5} \exp(-\gamma R_p / 18) \quad (1)$$

FIGURE 10

Experimental Distribution

Sample (a)

This is the experimental distribution of cosmic ray events as gathered by the Fly's Eye. It consists of 1137 events gathered in 800 hours of running, each event having $R_p > 1.0$ km and $\Delta\theta > 50^\circ$ (excluding those tubes with $\theta_i < 20^\circ$).

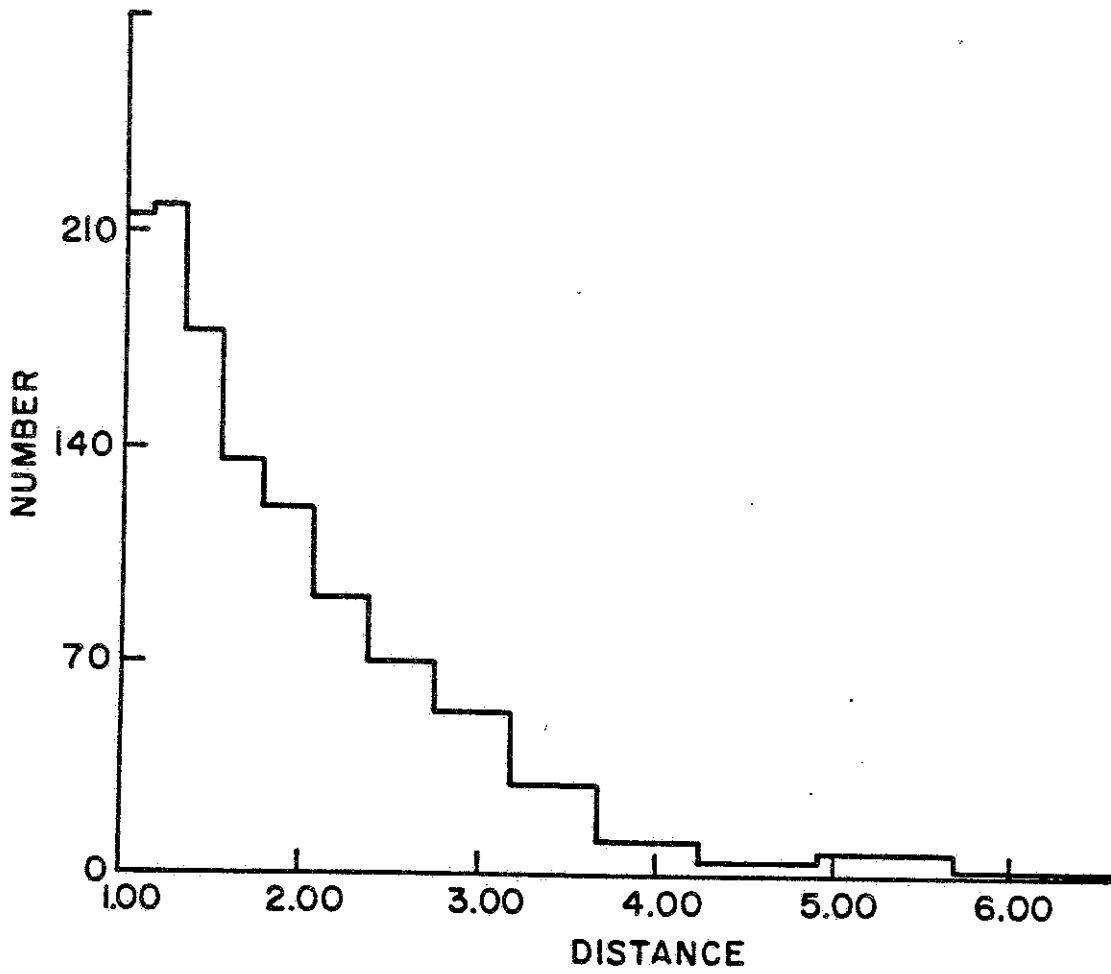


FIGURE 11

Experimental Distribution

Sample (b)

This distribution of 397 events is a subset of sample (a) (see Figure 10). For this distribution we required $R_p > 1.0\text{km}$ and $\Delta\theta > 70^\circ$, with no cut on initial viewing angle.

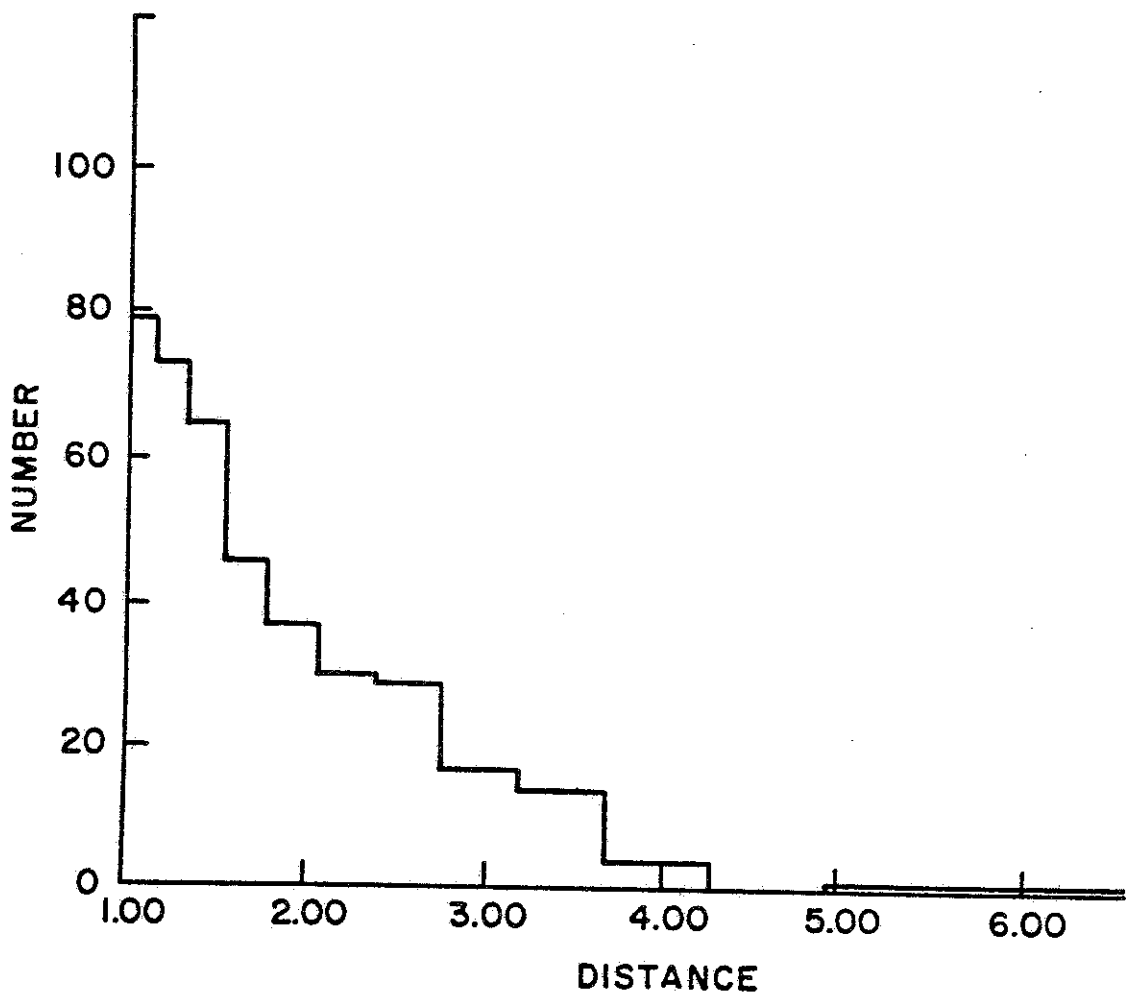


FIGURE 12

Event with Cherenkov "Blast"
at Beginning

This figure is analogous to what would be seen on the event display (see Figure 8). The initial viewing angle (θ_1) for this shower is approximately one degree. Geometrical reconstruction only gives R_p to within 50% ($R_p=0.5\pm 0.25$ km).

FILE 9-4-1
EVENT 93

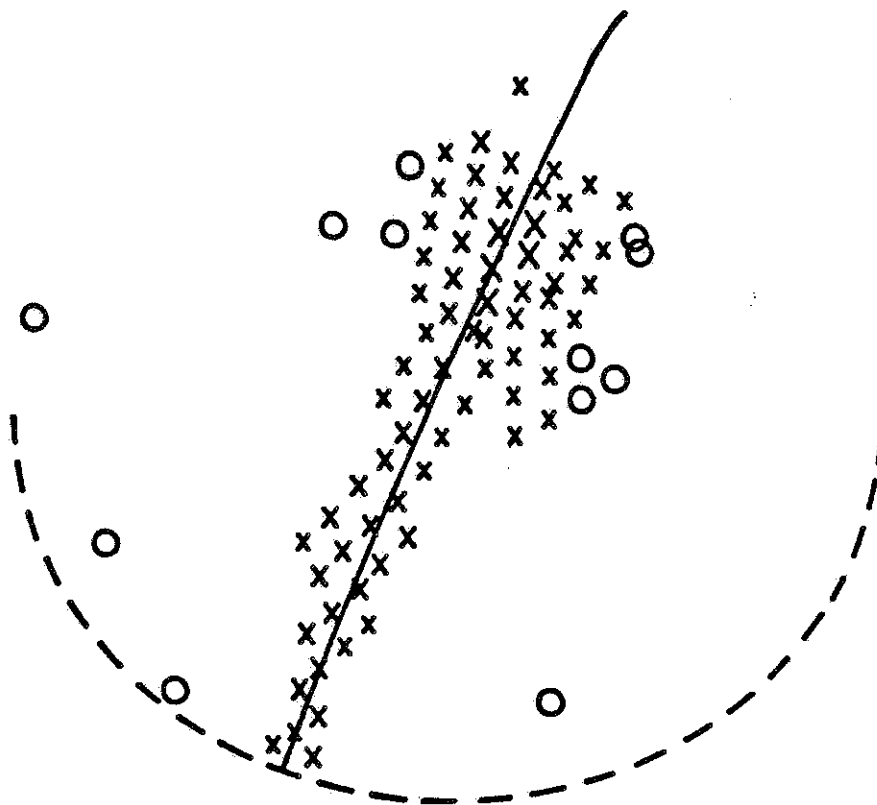
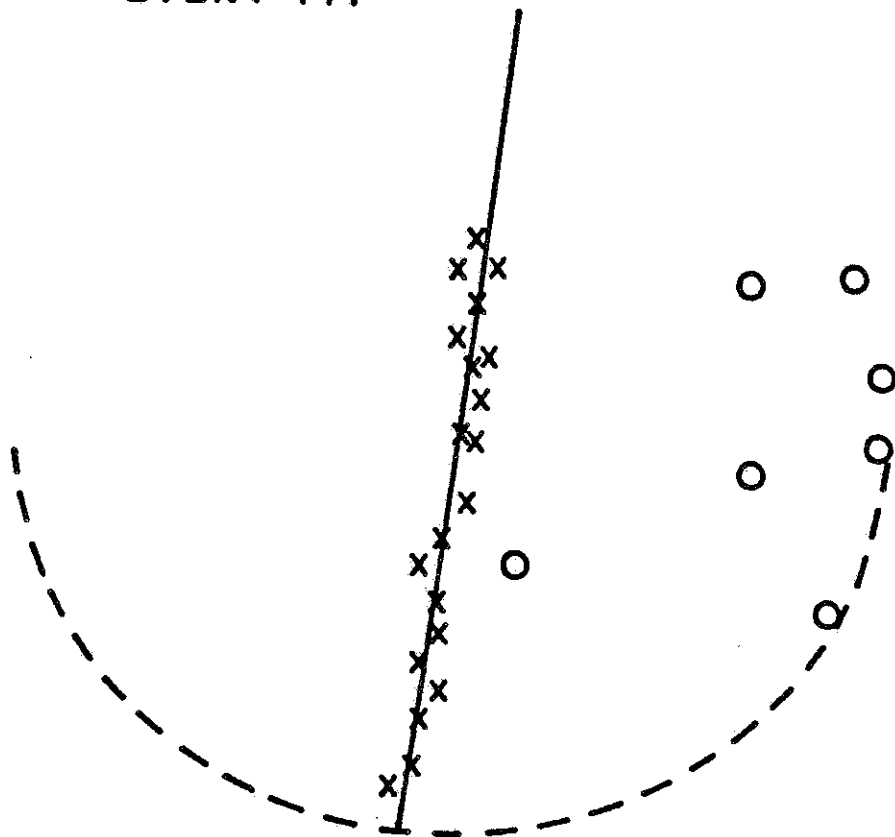


FIGURE 13

Well Reconstructed Event

Initial viewing angle is approximately 17° . Impact parameter known to within 5% ($R_p=2.1\pm 0.1$ km).

FILE 9-14-3
EVENT 147



to the first nine bins of the data of sample (b). The results, shown in Figure 14, gave a spectral index of 2.1 ± 0.3 , well within the the range of previous results. The derivation of the fitting function is given below.

Assume the light output of the shower as gathered by the Fly's Eye varies as $1/R_p$ (the shower is a line source). If T is the integrate time for a given integration channel then the size of the fluctuations in the integrated signal due to background light will go as $1/\sqrt{T}$. Since the pulse width in a tube, and therefore the channel which will trigger for a given shower, varies as R_p , the trigger voltage that the discriminator is set at will go as $1/\sqrt{R_p}$, so that the channel will be set for maximum sensitivity without triggering on too many noise pulses. Therefore the energy of a shower that will barely trigger the detector will vary as $R_p^{1.5}$, neglecting scattering. Including Rayleigh scattering, we get the energy of a shower that will barely trigger the detector going as $E \propto R_p^{-1.5} \exp(-R_p/18)$ (where 18 km is the Rayleigh scattering length for light of wavelength 400 nm). By multiplying by an undetermined constant, we can convert this into an equality. If we substitute this equality into the rate equation $I(>E)$, and allow the constant to also convert rate to number, we get:

$$dN/dR_p = C \cdot R_p^{-1.5} \exp(-R_p/18) \quad (2)$$

where C is the undetermined constant. Since the bin size (dR_p) is $R_p \pm 7.8\%$, the number (dN) of events in a given R_p bin can be written:

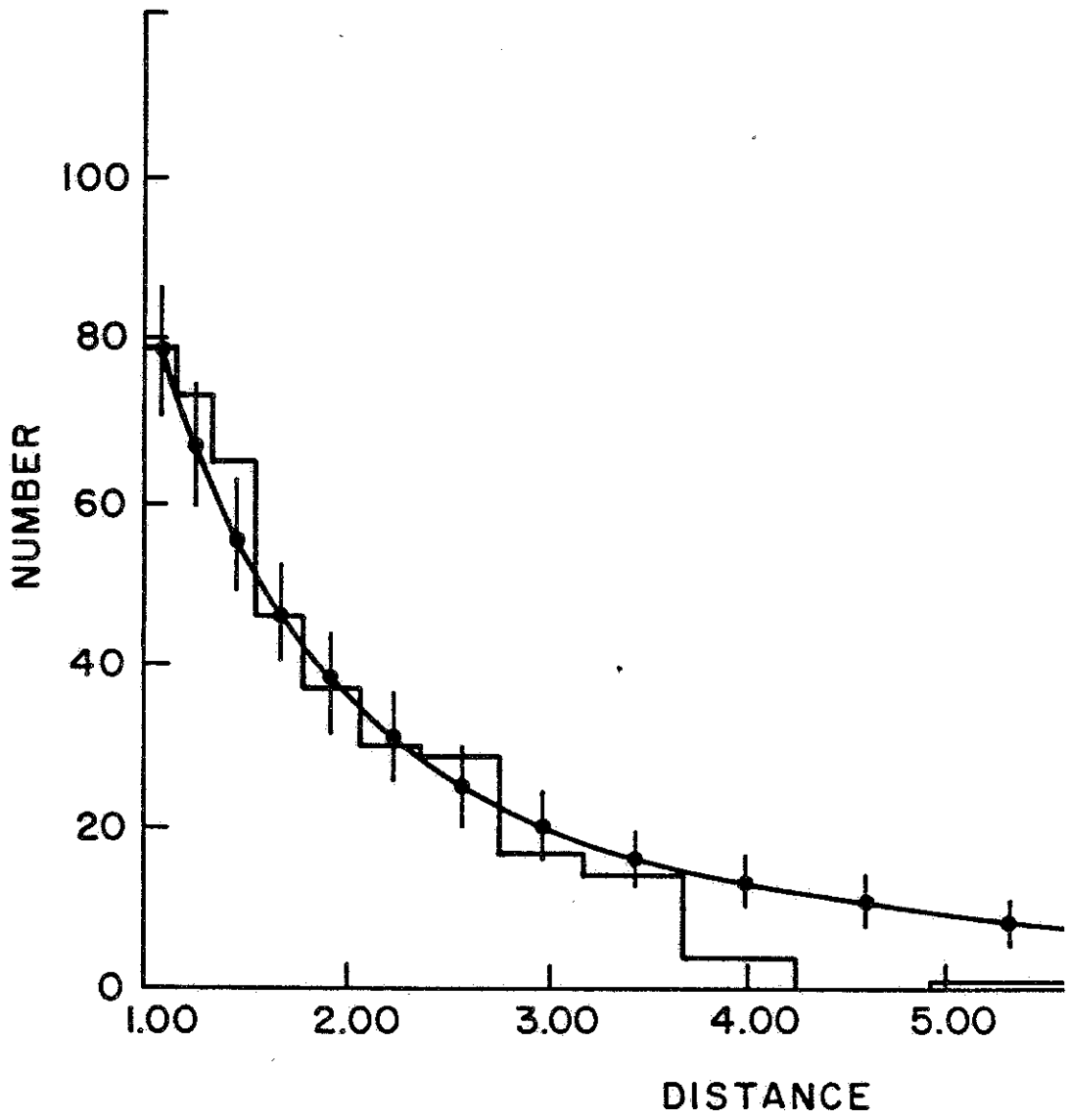
$$dN = D \cdot R_p^{-2.5} \exp(-R_p/18) \quad (3)$$

where D is another undetermined constant. Since C is not known,

FIGURE 14

Simple Parametric Fit to
Sample (b)

Best fit given for $\gamma=2.1\pm.3$, using only the first nine bins. Error bars show statistical errors ($\pm 1\sigma$ binomial) for each bin. The line joining the points of the parametric fit is only there to guide the eye.



the value of D is just a fitting parameter containing no information.

5.3 Simulation Fit

Fits of the simulated distributions generated by SPECSM to the Fly's Eye data are shown in Figures 15 and 16. The data shown in Figure 15 are those of sample (a). The fit gave a spectral index of 1.99 ± 0.04 , and a normalization $A = (1.92 \pm 0.12) \times 10^{-10} \text{ m}^{-2} \cdot \text{sec}^{-1} \cdot \text{str}^{-1}$ where the quoted errors are fitting errors only. For Figure 16, using the data of sample (b), the fit gave $\gamma = 2.03 \pm 0.10$ and $A = (2.43 \pm 0.43) \times 10^{-10} \text{ m}^{-2} \cdot \text{sec}^{-1} \cdot \text{str}^{-1}$. Note that the range of values fit to sample (b) overlaps the range of values fit to sample (a). Since sample (b) was picked to determine the effects of the fit of more stringent geometrical cuts, this overlap suggests that being more restrictive will not improve our results. However, reconstructions of simulated events by GEO suggest that there are systematic errors in reconstructing short track length, small initial viewing angle events, so we would expect that being less restrictive would affect our results, as indeed it does.

5.4 Comparison with Results of Others

The table below summarizes the best current results on the cosmic ray energy spectrum, along with the results of this work:

| Experiment | γ | A |
|---------------------------|-----------------|-----------------------------------|
| Haverah Park ³ | 2.05 ± 0.02 | 2.6×10^{-10} |
| Yakutsk ²¹ | $2.05 \pm ?$ | 1.7×10^{-10} |
| Sydney ³⁷ | 2.00 ± 0.02 | ? |
| Sample (a) | 1.99 ± 0.04 | $(1.92 \pm 0.12) \times 10^{-10}$ |
| Sample (b) | 2.03 ± 0.10 | $(2.43 \pm 0.43) \times 10^{-10}$ |

FIGURE 15

Simulation Fit to Sample (a)

Best fit gives $\gamma=1.99\pm.04$ and $A=(1.92\pm.12)\times 10^{-10} \text{ m}^{-2}\cdot\text{sec}^{-1}\cdot\text{str}^{-1}$. Quoted errors are those of fitting only. Errors due to geometrical reconstruction, errors in measuring the on time of the detector, etc., are not treated.

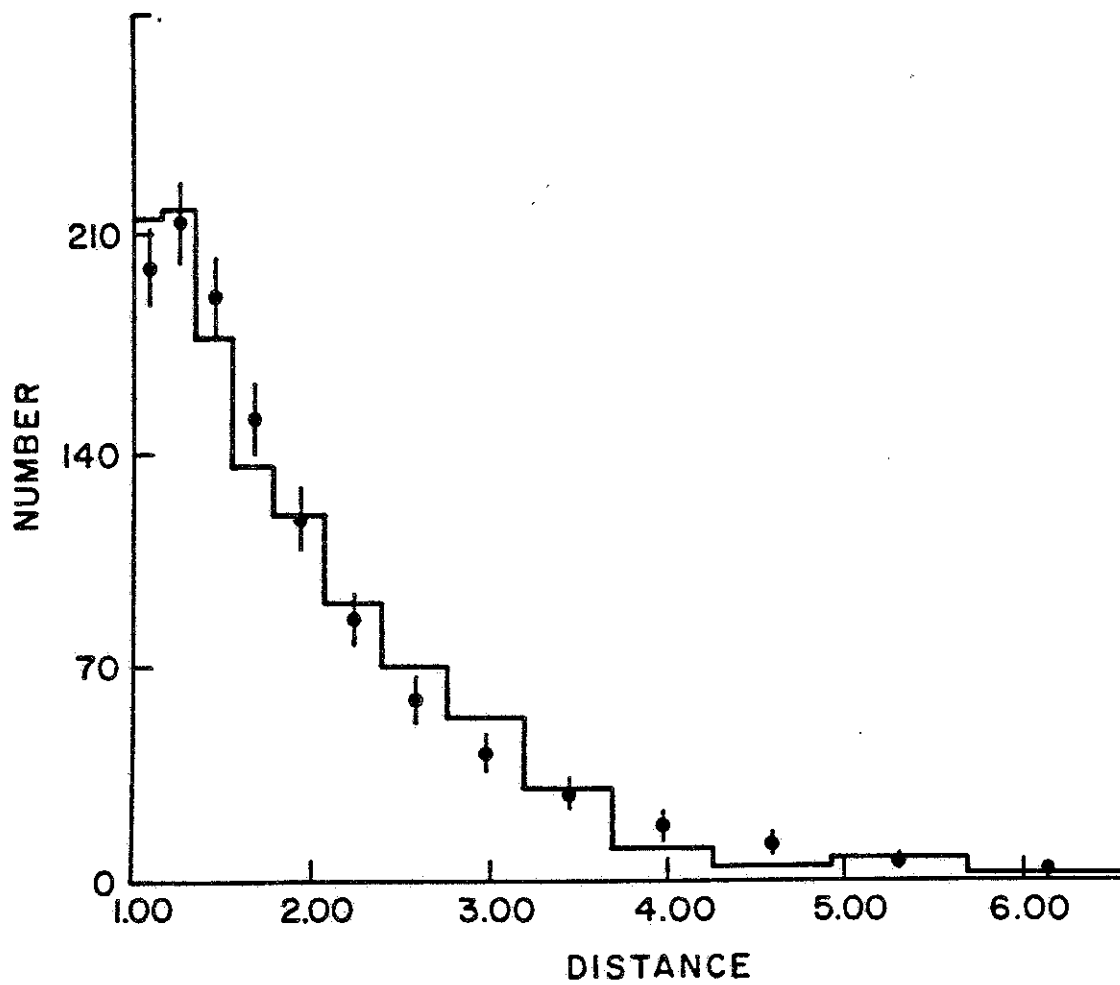
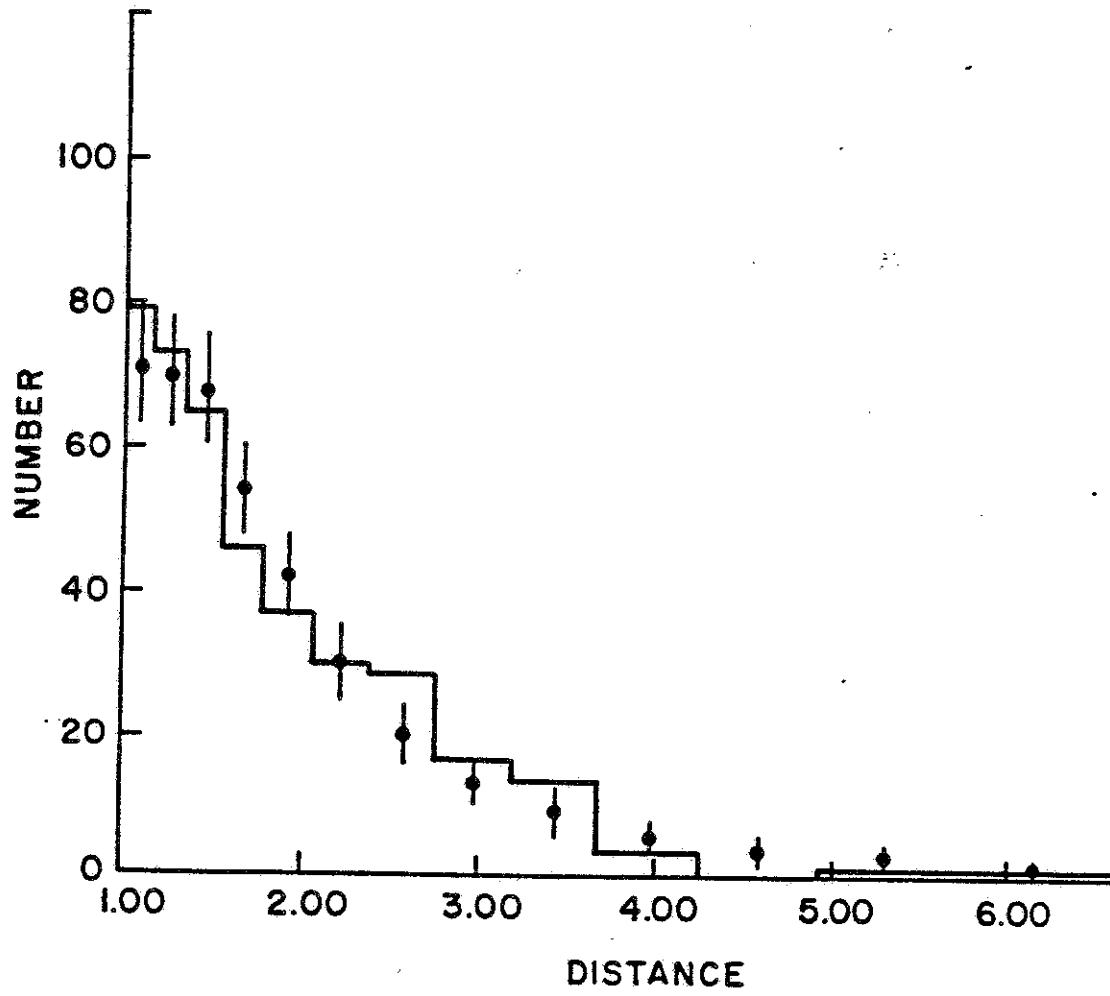


FIGURE 16

Simulation Fit to Sample (b)

Best fit gives $\gamma=2.03\pm.10$ and $A=(2.43\pm.43)\times 10^{-10}\text{m}^{-2}\cdot\text{sec}^{-1}\cdot\text{str}^{-1}$



As can be seen, the Fly's Eye results overlap those of the other groups for the spectral index. For the more difficult to measure normalization A, the values given by the Fly's Eye fall right between the results of the other groups.[†] So on the whole, the results of this method of interpreting the data of the Fly's agrees with the results of others on the cosmic ray integrated energy spectrum.

[†] Note that values for A were not quoted in the recent literature. I calculated these values by measuring them off of a graph⁴ (see Figure 1).

LIST OF REFERENCES

- 1 Hillas A. M., Cosmic Rays, Oxford, New York, Pergamon Press, (1972).
- 2 Cutler D. J. et al., "Measurement of the Cosmic-Ray Sidereal Anisotropy near 1500 GV," Ap. J., 248, 1166 (1981)
- 3 Bower A. J. et al., "On Estimating the Energy of Giant Air Shower Primaries," submitted for publication J. Phys. G, 22 October, 1982.
- 4 Hillas A. M., "Observations on the Energy Spectrum, Composition, and Anisotropy of Primary Cosmic Rays above 1000 GeV," Conference Papers, 17th ICRC, 13, 69 (1981).
- 5 Fermi E., "On the Origin of Cosmic Radiation," Phys Rev, 2nd Ser, 75, 1169 (1949).
- 6 Grigorev N. L., "The Abundances of Cosmic Ray Nuclei," Conference Papers, 12th ICRC, 1, 170 (1971).
- 7 Ogata T. et al., "Chemical Composition of Cosmic Rays at Energies greater than 10^{13} eV," Conference Papers, 17th ICRC, 2, 119 (1981).
- 8 Hinshaw G. F. et al., "A Study of Galactic Cosmic Ray Propagation Models based on the Isotopic Composition of the Elements Lithium, Beryllium, and Boron," Conference Papers, 17th ICRC, 9, 191 (1981).
- 9 Wiedenbeck M. E. and Greiner D. E., "A Cosmic Ray Age based on the Abundance of ^{10}Be ," Ap. J., 239, L139 (1980).
- 10 Cowsik R. and Lee M. A., "Simple Analytic Solutions Appropriate for Galactic Cosmic Ray Modulation," Ap. J., 216, 635 (1977).
- 11 Blandford R. D. and Ostriker J. P., "Particle Acceleration by Astrophysical Shocks," Ap. J., 227, L49 (1978).
- 12 Axford W. I., "Acceleration of Cosmic Rays by Shock Waves," Conference Papers, 17th ICRC, 12, 155 (1981).
- 13 Volk H. J., "Cosmic Ray Sources: II Acceleration," Conference Papers, 17th ICRC, 13, 131 (1981).

- 14 Michel F. C., "Theory of Pulsar Magnetospheres," *Rev Mod Phys.*, 54, 1 (1982).
- 15 Berezhinsky V. S. and Grigor'eva S. I., "Cosmic Rays from the Local Supercluster: Sources and Spectra," *Conference Papers, 16th ICRC*, 2, 81 (1979).
- 16 Wdowczyk J. and Wolfendale A. W., "Origin of the Highest Energy Cosmic Rays," *Conference Papers, 16th ICRC*, 2, 154 (1979).
- 17 Greisen K., "End to the Cosmic Ray Spectrum?," *Phys. Rev. Lett.*, 16, 748 (1966).
- 18 Balick B. and Heckman T. M., "Spectroscopy of the Fuzz Associated with Four Quasars," *Ap. J.*, 265, L1 (1983).
- 19 see for example Cowsik R., "Properties of Air Showers and the Nature of the Primary Cosmic Ray Spectrum," *Can. J. Phys.*, 46, S142, (1968).
- 20 Watson A. A., "Cosmic Ray Anisotropy: 10^{12} - 10^{21} eV," *Proceedings of the XVth Rencontre de Moriond, Astrophysics* (1981).
- 21 See also ref 4; Efimov et al., title unknown, *Bull. Sci. Inf. Acad. Sci. USSR, Yakutsk*, August (1981).
- 22 Linsley J., "Large Air Showers and the Dust Grain Hypothesis," *Conference Papers, 17th ICRC*, 2, 141 (1981).
- 23 Sokolsky P., private communication (1982).
- 24 McComb T. J. L. et al., "Photoproduction in Large Cosmic Ray Showers," *J. Phys. G*, 5, 1613 (1979).
- 25 Linsley J. and Watson A. A., "Cosmic Ray Mass Composition above 10^{15} eV," *Conference Papers, 17th ICRC*, 2, 137 (1981).
- 26 Thornton G. and Clay R., "Development of Atmospheric Cosmic-Ray Showers," *Phys. Rev. Lett.*, 43, 1622 (1979).
- 27 Gaisser T. K. et al., "Cosmic Ray Showers and Particle Physics at Energies 10^{15} - 10^{18} eV," *Rev. Mod. Phys.*, 50, 859 (1978).
- 28 La Pointe et al., "Notes on the Primary Energy Spectrum of Cosmic Rays," *Can. J. Phys.*, 46, S68 (1968).
- 29 Linsley J., "Interpretation of Air Shower Data Relevant to Cosmic-Ray Composition," *Conference Papers, 15th ICRC*, 8, 431 (1977).